NASA TECHNICAL NOTE

NASA TN D-5694

NASA TN D-5694

HEAT TRANSFER AND LEVITATION OF A SPHERE IN LEIDENFROST BOILING

by Robert C. Hendricks and Kenneth J. Baumeister

Lewis Research Center
Cleveland, Ohio 44135

NATIONAL AERONAUTICS AND SPACE ADMINISTRATION • WASHINGTON, D. C. • JULY 1970

1. Report No. NASA TN D-5694	2. Government Accession No.	3. Recipient's Catalog No.
4. Title and Subtitle HEAT TRANSFER AND LEVITATION OF A SPHERE IN LEIDENFROST BOILING		5. Report Date July 1970 6. Performing Organization Code
7. Author(s) Robert C. Hendricks and Kenneth J. Baumeister		8. Performing Organization Report No. E-4109
9. Performing Organization Name and Address Lewis Research Center National Aeronautics and Space Administration Cleveland, Ohio 44135		10. Work Unit No. 129-01 11. Contract or Grant No. 13. Type of Report and Period Covered Technical Note
12. Sponsoring Agency Name and Address National Aeronautics and Space Administration Washington, D.C. 20546		14. Sponsoring Agency Code

15. Supplementary Notes

Film Supplement C-267 available on request.

16. Abstract

The heat-transfer coefficients are predicted for liquid or solid spheres supported in film boiling on a liquid surface (liquid-liquid and solid-liquid film boiling, respectively). For the case of water spheres on a liquid-nitrogen surface, the predicted freezing times compare favorably with experimental measurements.

17. Key Words (Suggested by Author(s))	18. Distribution Statement
Heat transfer Film boiling Leidenfrost Levitation	Unclassified - unlimited

19. Security Classif. (of this report)	20. Security Classif. (of this page)	21. No. of Pages	22. Price*
Unclassified	Unclassified	94	$3.00

*For sale by the Clearinghouse for Federal Scientific and Technical Information Springfield, Virginia 22151

CONTENTS

HEAT TRANSFER AND LEVITATION OF A SPHERE IN LEIDENFROST BOILING

by Robert C. Hendricks and Kenneth J. Baumeister

Lewis Research Center

SUMMARY

A hydrodynamic model is postulated for a small, spherical, liquid drop film boiling on a cryogenic surface, such as may occur in propellant spillage accidents and in the preparation and preservation of some biological species (e.g., blood and enzymes). The momentum and energy equations are solved analytically to predict the velocity and temperature fields in the vapor film beneath the sphere. This leads to a heat-transfer coefficient of the form

$$h_d = \frac{k}{R_o} + \kappa\left[\frac{k^3 \rho_d \rho g \lambda^*}{R_o \mu (T_d - T_s) F(\theta^*)}\right]^{1/4}$$

where k is the thermal conductivity of the vapor, ρ_d the density of the sphere, ρ the density of the vapor, λ^* the modified latent heat, R_o the radius of the sphere, μ the vapor viscosity, T_d and T_s the temperature of the sphere and the liquid, respectively, κ a constant, and $F(\theta^*)$ a function which depends on the characteristics of the sphere and the supporting fluid. The values of κ and $F(\theta^*)$ and dimensionless forms of the heat-transfer solutions are given in the body of the report (see table II).

This expression for the heat-transfer coefficient combined with a thermal balance predicts the time necessary for spheres at room temperature (liquid-liquid film boiling) to freeze when placed on a cryogenic liquid (solid-liquid film boiling). The agreement between experimental and predicted times is fair. A more extensive freezing analysis and thermocoupled spheres appear to be necessary.

Two solutions for the heat-transfer coefficient between the drop and the supporting surface are presented herein, one for a variable vapor-gap thickness and the other for constant vapor-gap thickness. These solutions and their associated boundary conditions at the liquid-vapor interface revealed two significant facets: (1) Whether the analyst assumes a constant or variable vapor-gap thickness, the resulting average heat-transfer coefficients are not significantly different; and (2) a technique called the integral boundary constraint can be used to handle undesirable nonconstant boundary conditions.

INTRODUCTION

Film-boiling heat transfer between two liquids at different temperatures has been under extensive investigation recently in consideration of propellant spillage accidents (ref. 1). If liquid propellants spill accidently during test-stand or launching operations, a catastrophic explosion resulting from the detonation of the fuel and oxidizer is possible. In particular, a number of experiments (ref. 1) have been performed involving the mixing of small kerosene spheres in liquid oxygen. When small kerosene spheres are dispersed in a matrix of liquid oxygen, the sensible heat of the kerosene spheres vaporizes the liquid oxygen, thereby forming a film of oxygen vapor around the sphere. This vapor film has a significant damping effect on the mixture's explosive potential, since gaseous oxygen contacting the liquid fuel has a much lower explosive potential than concentrated liquid oxygen.

The liquid-liquid film-boiling phenomenon is also of interest purely from stability considerations. In this case, a liquid sphere with a higher specific gravity floats upon a a cryogenic liquid of lower specific gravity while film boiling is taking place. The sphere usually freezes and continues to float (solid-liquid film boiling); suddenly at the transition from film boiling to nucleate boiling, the vapor blanket surrounding the sphere disappears. Then the sphere sinks beneath the liquid and falls to the bottom of the pool.

This report considers two aspects of this liquid-liquid film-boiling problem. First, a hydrodynamic model is postulated for a small, spherical, liquid drop film boiling on a cryogenic surface. The conservation equations of momentum and energy are solved analytically to predict the velocity and temperature fields, and a simple theoretical correlation for the heat-transfer coefficient is presented.

Actually, two solutions are presented, one for the case of variable vapor-gap thickness, which is limited to $\theta^* < \pi/2$ (see fig. 1); and the other more general solution for an assumed constant vapor-gap thickness, which is valid for $\theta^* < \pi$. The angle θ^* is the interface separation angle, that is, the angle from the stagnation point to where the sphere and the interface separate. This angle is discussed in detail in the next section. Two completely different similarity transforms are used to obtain the different solutions; and, to attain an exact solution to the variable-vapor-gap problem, a technique of conditioning the boundaries called the integral boundary constraint is used.

Both solutions, however, are shown to yield expressions for the heat-transfer coefficient which differ only by a constant which is much smaller than can be detected by our experiment. The agreement between the two solutions gives some credence to the almost universal assumption of constant vapor-gap thickness in solving film-boiling problems (refs. 2 to 4).

Secondly, a heat balance is performed on the sphere, which leads to a correlation equation for predicting the time required for a liquid sphere to cool from room tempera-

ture to its freezing point and then to the temperature at which boiling ceases; liquid subcooling was neglected. Theory is checked with experiment by placing water spheres on liquid nitrogen and comparing the experimental and theoretically predicted times for the liquid sphere to freeze. Fair agreement was found.

A motion-picture supplement C-267 has been prepared and is available on loan. The film supplement demonstrates and discusses the phenomena associated with levitated spheres in Leidenfrost boiling. A request card and a description of the film are included at the back of this report.

BASIC MODEL AND EQUATIONS

Consider the film-boiling model depicted in figure 1. This model appears to fit the

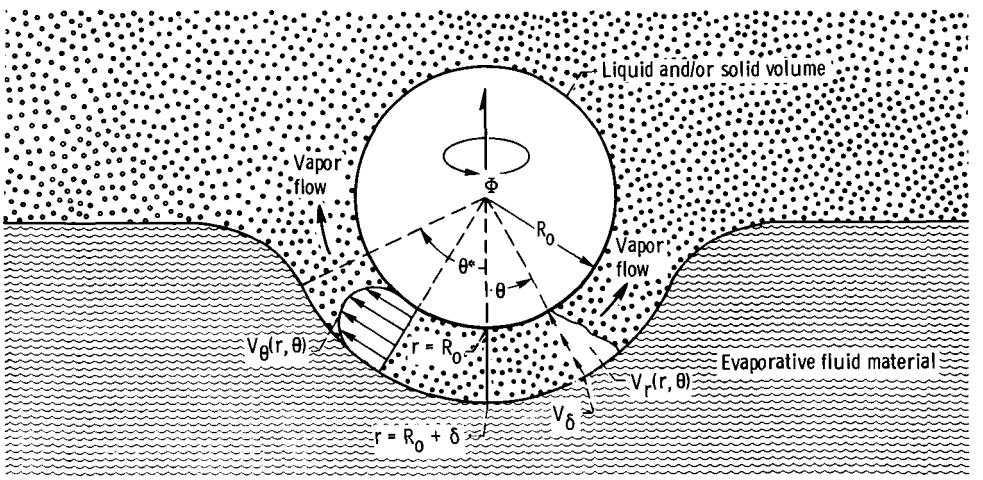

Figure 1. - Schematic model for evaporation from spherical interface.

physical case of a solid or liquid sphere "floating" on a second liquid (solid-liquid and liquid-liquid film boiling); for example, drops of water floating on a sea of liquid nitrogen. There is, of course, no reason to limit the model to liquid spheres or cryogenic fluids. Slush and small solid materials could also be utilized on any liquid provided the proper temperature difference and buoyancy criteria are maintained.

The model used in this study applies to two cases with spherical geometries:

(1) In the first case, the vapor-gap thickness for a floating sphere is permitted to vary, although the subsequent solution is limited to $\theta^* < \pi/2$. Such a solution seems to model the physical process quite well. However, some difficulties are encountered, and the limitation to $\theta^* < \pi/2$ is too constrained. It will be shown that the average heat-

transfer coefficient for the variable-vapor-gap case vindicates the assumption of constant vapor-gap thickness; however, the authors sought another solution to the problem, which is applicable to $\theta^* < \pi$.

(2) The second case, which assumes a constant vapor-gap thickness, sacrifices some of the physics (e.g., the variable gap thickness) in return for a solution which is applicable for $\theta^* < \pi$.

The consideration of these two cases requires different similarity transforms, as discussed in the section Similarity Transforms. The model may be applied either to the case where the sensible heat of the floating sphere evaporates the encompassing liquid or to the case where the sensible heat of the encompassing liquid evaporates the floating sphere (e.g., liquid-nitrogen sphere on water). For simplicity, it is assumed throughout the remainder of this report that the supporting fluid evaporates at the interface. Physically, for the experimental results considered herein, the heat passes from the warmer spherical drop and evaporates the fluid material beneath it, thereby forming a supporting vapor layer under the sphere. The vapor layer is, in turn, supported by the interface. Surface tension, density ratio, buoyancy, surface curvature, and the "nonwetting" character of the interface play an important role in determining whether the interface is strong enough to support the sphere. During the evaporative, or film-boiling, process the temperature of the sphere decreases until it coincides with the Leidenfrost temperature of the liquid. At this time, film boiling ceases, and transition boiling quickly followed by nucleate boiling begins. The vapor layer beneath the sphere no longer exists; rather, small nucleate bubbles form in the sites on the solid (liquid) sphere. Thus, because there is no longer a supporting vapor gap, the sphere sinks beneath the surface and falls to the bottom.

The following assumptions are made in developing the model:

(1) Evaporation and internal circulation of the liquid sphere are considered to be small.

(2) The model has complete symmetry with respect to the angular coordinate Φ.

(3) The flow of vapor is considered to be laminar and incompressible; and the inertia terms in the Navier-Stokes equations are neglected. Justification for this assumption can be found in reference 2.

(4) Radiation is assumed to be negligible.

(5) The velocity and temperature profiles are assumed to be in steady state.

(6) At any instant of time, the sphere is at an average temperature $\overline{T}_d$, and the evaporating liquid is assumed to be at the saturation temperature T_s. The properties of the flow field are evaluated at the film temperature

$$T_f = \frac{\overline{T}_d + T_s}{2}$$

and are considered to be constant. This assumption has worked quite well (e.g., ref. 5). (All symbols are defined in appendix A.)

(7) The convective terms in the energy equation, as treated in appendix F, effect a correction factor on the conduction term. The correction factor is taken to be 1 (i.e., conduction dominates) to make the problem tractable. Such an assumption is apparently a good one based on the work in references 2, 5, and 6. These authors indicate the major mode of heat transport to be conduction, as further verified in appendix F. Thus, it is assumed that

$$\frac{V_\theta}{r}\frac{\partial T}{\partial \theta} < V_r \frac{\partial T}{\partial r} \ll \frac{k}{\rho C_p r^2}\frac{\partial}{\partial r}\left(r^2 \frac{\partial T}{\partial r}\right) \tag{1}$$

$$\frac{1}{r^2 \sin\theta}\frac{\partial}{\partial \theta}\left(\sin\theta \frac{\partial T}{\partial \theta}\right) < \frac{1}{r^2}\frac{\partial}{\partial r}\left(r^2 \frac{\partial T}{\partial r}\right) \tag{2}$$

(8) Heat transport within the sphere is by conduction alone. With cooling at the lower surface, there should be no instabilities or ensuing cellular motion.

(9) The supporting liquid is at the saturation temperature. Thus, with assumption 7, all the heat reaching the liquid produces vapor.

(10) Subcooling of the liquid sphere was considered but omitted because of the presence of the freezing crystalline ice shell.

Governing Equations

The governing equations are as follows (ref. 7):

Momentum:

$$0 = \frac{-g_c}{\rho}\frac{\partial P}{\partial r} + \nu\left(\nabla^2 V_r - \frac{2V_r}{r^2} - \frac{2}{r^2}\frac{\partial V_\theta}{\partial \theta} - \frac{2}{r^2} V_\theta \cot\theta\right) \tag{3}$$

$$0 = \frac{-g_c}{\rho}\frac{1}{r}\frac{\partial P}{\partial \theta} + \nu\left(\nabla^2 V_\theta + \frac{2}{r^2}\frac{\partial V_r}{\partial \theta} - \frac{V_\theta}{r^2 \sin^2\theta}\right) \tag{4}$$

where

$$\nabla^2 = \frac{1}{r^2}\frac{\partial}{\partial r}\left(r^2\frac{\partial}{\partial r}\right) + \frac{1}{r^2 \sin\theta}\frac{\partial}{\partial\theta}\left(\sin\theta\frac{\partial}{\partial\theta}\right) \tag{5}$$

Energy:

$$0 = \frac{\partial}{\partial r}\left(r^2\frac{\partial T}{\partial r}\right) \tag{6}$$

Continuity:

$$0 = \frac{1}{r^2}\frac{\partial}{\partial r}(r^2 V_r) + \frac{1}{r\sin\theta}\frac{\partial}{\partial\theta}(V_\theta \sin\theta) \tag{7}$$

The boundary conditions on the velocity and temperature fields are given in table I, where θ^* is defined in figure 1, and δ is the vapor-gap thickness.

TABLE I. - BOUNDARY CONDITIONS FOR FLOATING SPHERE

Area	Surface	Boundary condition	Equation number
Sphere surface	$r = R_o$ $\theta \leq \theta^*$	$V_r = 0$ $V_\theta = 0$ $T = T_d - \epsilon(T_d - T_s)\cos\theta$	(8)
Liquid-vapor interface	$r = R_o + \delta$ $\theta \leq \theta^*$	$V_r = V_r(\delta)$ $V_\theta = 0$ $T = T_s$	(9)
Stagnation region	$R_o \leq r \leq R_o + \delta$ $\theta = 0$	$V_\theta = 0$	(10)
Separation region	$r = R_o$ $\theta = \theta^*$	$P = P_o$	(11)

The tangential V_θ and radial V_r vapor velocities are both zero at the surface of the sphere (eq. (8)), while only the tangential velocity V_θ is zero at the surface of the cryogenic supporting liquid (eq. (9)). Because of evaporation, a radial velocity $V_r(\delta)$ exists at the surface of the cryogenic fluid.

The cryogenic fluid is assumed to be at the saturation temperature T_s, as shown in equation (9). The boundary condition at the surface of the sphere is more complicated and, in fact, an unknown. In this report, the general case of a surface temperature of the form

$$T = T_d - \epsilon(T_d - T_s) \cos \theta \tag{11a}$$

is investigated. Specifically, two cases are considered:

(i) The sphere is assumed to be at an average temperature, a condition discussed more fully in the section Integral average constraint (p. 9); that is, using equation (11) and integrating over the surface of the sphere,

$$\overline{T}_d = \frac{1}{A} \int_A T \, dA = T_d \tag{11b}$$

(ii) The temperature at the surface of the sphere follows a cosine variation with some assumed value of ϵ (a positive constant which is less than 1). This is investigated for the first case only (i.e., when $\theta^* < \pi/2$).

Constraints

The boundary conditions are still incomplete at this point since $V_r(\delta)$, δ, and θ^* are unknowns. Hence, three additional mathematical constraints are necessary to make the problem tractable. A fourth mathematical constraint is required in the case of the variable vapor-gap thickness to force a tractable solution.

Static force balance (neglecting forces internal to sphere). - One additional constraint requires the sphere to be in static equilibrium. Small vibrations of the sphere are neglected. The static equilibrium condition requires that the weight of the sphere be balanced by the shear and pressure forces acting beneath the sphere. These forces are depicted in figure 2. Summing the forces acting in the vertical direction gives

$$0 = W_d - \int_0^{2\pi} \int_0^{\theta^*} (P \cos \theta + \tau_{r\theta} \sin \theta - \tau_{rr} \cos \theta)\Big|_{r=R_o} R_o^2 \sin \theta \, d\theta \, d\Phi$$

$$- \int_0^{2\pi} \int_{\theta^*}^{\pi/2} P_o \cos \theta \, R_o^2 \sin \theta \, d\theta \, d\Phi + \pi R_o^2 P_o \tag{12}$$

The last two terms in equation (12) represent ambient pressure forces acting on the sphere.

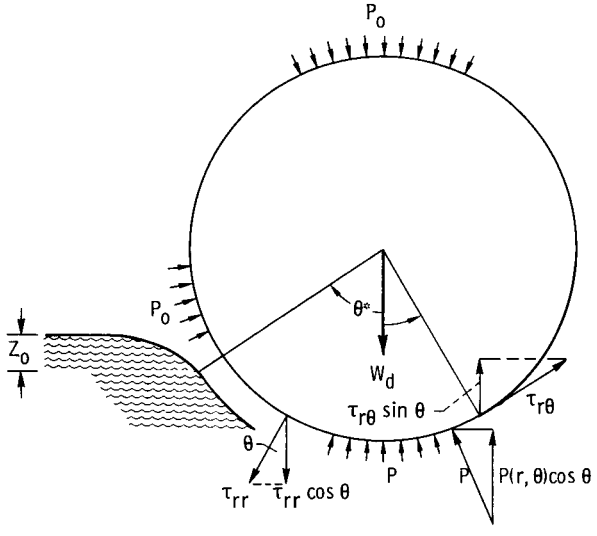

Figure 2. - Schematic model of pressure and shear forces acting on sphere.

Interface energy balance. - The second constraint necessary for the solution of equations (3) to (7) is the interface energy balance. Because the supporting fluid has been assumed to be at the saturation temperature (assumption 9), all the heat leaving the sphere produces evaporation of the fluid material. Mathematically, this constraint is expressed as

$$-\rho\lambda V_r(R_o + \delta, \theta) = -k \left.\frac{\partial T}{\partial r}\right|_{r=R_o+\delta} \tag{13}$$

where λ is the latent heat of vaporization and $-k \left.\frac{\partial T}{\partial r}\right|_{r=R_o+\delta}$ is the conduction heat flux to the boundary of the supporting liquid.

Free-surface pressure head. - The third constraint is that the forces supporting the sphere must be transmitted and balanced by the supporting fluid interface. Here the free-surface heat Z_o, as shown in figure 2 (see also fig. 8), must be determined from a balance of forces acting on the liquid-vapor surface membrane. The determination of Z_o such that all forces are balanced and the sphere is supported also uniquely prescribes a value to θ^*. The solution for Z_o is discussed in appendix H.

Integral average constraint. - A fourth constraint which the authors found to be a very valuable tool in solving problems with nonconstant boundary conditions is constraining the problem to satisfy a suitably averaged condition at the boundary. While the technique has general applicability, the constraint was used for the following two cases. First, for the variable-vapor-gap case, it was found that in order to make the problem rigorous, the radial velocity at the liquid-vapor interface had to be a suitable average value if the surface temperature was assumed to be constant. Employing the integral average constraint yields

$$\overline{V}_{\delta} = \frac{1}{A} \int_{A} V_r(\delta, \theta)\, dA \tag{13a}$$

In similar manner, the average surface temperature is defined by using equation (11) and the integral average constraint

$$\overline{T} = \frac{1}{A_1} \int_{A_1} T(1, \theta)\, dA_1 \tag{13b}$$

where A_1 is not necessarily equal to A, a choice which is available to the analyst. For example, A_1 could represent only the area influenced by the vapor ($0 \leq \theta \leq \theta^*$), in which case

$$\overline{T}_d = \frac{\int T\, dA}{A} = \frac{2\pi \int (T_d - \epsilon\, \Delta T \cos\theta) R_o^2 \sin\theta\, d\theta}{2\pi \int R_o^2 \sin\theta\, d\theta}$$

$$\overline{T}_d = T_d - \frac{\epsilon\, \Delta T}{2}(1 + \cos\theta^*) \tag{13c}$$

If, however, the analyst chooses $A = A_1$ ($0 \leq \theta \leq \pi$), then $\overline{T}_d = T_d$.

The solution of the preceding set of differential equations is given in the next section. Figure 3 presents a solution flow chart of the problem, which may be used as a study aid.

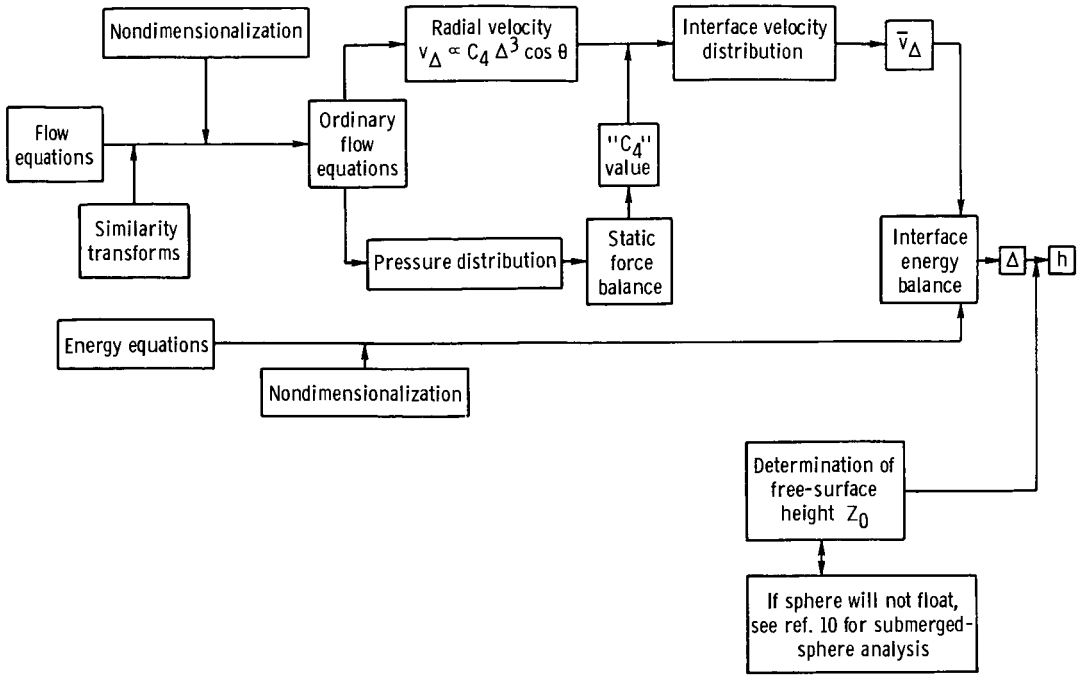

Figure 3. - Solution flow chart.

SOLUTION

Momentum Equations

The governing equations are made nondimensional to generalize the solution by selecting the following parameters:

$$\zeta = \frac{r}{R_o} \tag{14}$$

$$v_\zeta = \frac{V_r}{u^*} \tag{15}$$

$$v_\theta = \frac{V_\theta}{u^*} \tag{16}$$

$$u^* = \frac{\nu}{R_o} \tag{17}$$

$$Re = \frac{\rho u^* R_o}{\mu} \equiv 1 \tag{18}$$

$$p = \frac{P}{\frac{\rho u^{*2}}{g_c}} \tag{19}$$

Substituting these parameters into the momentum equations gives

$$0 = -\frac{\partial p}{\partial \zeta} + \nabla^2 v_\zeta - \frac{2}{\zeta^2} v_\zeta - \frac{2}{\zeta^2} \frac{\partial v_\theta}{\partial \theta} - \frac{2}{\zeta^2} v_\theta \cot \theta \tag{20}$$

$$0 = -\frac{1}{\zeta} \frac{\partial p}{\partial \theta} + \nabla^2 v_\theta + \frac{2}{\zeta^2} \frac{\partial v_\zeta}{\partial \theta} - \frac{v_\theta}{\zeta^2 \sin^2 \theta} \tag{21}$$

where

$$\nabla^2 = \frac{1}{\zeta^2} \frac{\partial}{\partial \zeta} \left(\zeta^2 \frac{\partial}{\partial \zeta} \right) + \frac{1}{\zeta^2 \sin \theta} \frac{\partial}{\partial \theta} \left(\sin \theta \frac{\partial}{\partial \theta} \right) \tag{22}$$

Introducting the stream function for spherical coordinates (ref. 7, p. 131) gives for the velocity distribution

$$V_r = -\frac{1}{r^2 \sin \theta} \frac{\partial \psi}{\partial \theta} \tag{23}$$

$$V_\theta = \frac{1}{r \sin \theta} \frac{\partial \psi}{\partial r} \tag{24}$$

or, in terms of the dimensionless velocities,

$$v_\zeta = -\frac{1}{\zeta^2 \sin \theta} \frac{\partial \psi(\zeta, \theta)}{\partial \theta} \tag{25}$$

$$v_\theta = \frac{1}{\zeta \sin \theta} \frac{\partial \psi(\zeta, \theta)}{\partial \zeta} \tag{26}$$

Substituting equations (25) and (26) into the momentum equations (eqs. (21) and (22)) and combining to eliminate the pressure terms give

$$E^4(\psi) = 0 \tag{27}$$

where

$$E^2 \equiv \frac{\partial^2}{\partial \zeta^2} + \frac{\sin \theta}{\zeta^2} \frac{\partial}{\partial \theta}\left(\frac{1}{\sin \theta} \frac{\partial}{\partial \theta}\right) \tag{28}$$

Similarity Transforms

The governing stream function differential equation (eq. (27)) is now reduced to an ordinary differential equation by means of similarity transforms. For the variable-vapor-gap-thickness case, the transform is

$$T_1: \qquad \psi_1(\zeta, \theta) = F_1(\zeta) \sin^2 \theta \tag{29}$$

which is restricted to those values of θ less than $\pi/2$. For the more general but less physically realistic case of constant vapor-gap thickness, the transform is

$$T_2: \qquad \psi_2(\zeta, \theta) = F_2(\zeta)(1 - \cos \theta) \tag{30}$$

For small spheres where the density ratio between the sphere and the supporting fluid is near 1, the value of θ^* is less than $\pi/2$. In this case, either transform gives approximately the same value of the heat-transfer coefficient. At present, which solution more nearly approximates the actual flow has not been determined.

For heavy or large-diameter spheres, however, θ^* is greater than $\pi/2$. In this case, only the second transformation can be used.

Heat-Transfer Coefficient

The details of the solution of the momentum equation and the energy equation are long and involved and are performed in the appendixes.

By using the similarity transform T_1 (eq. (29)), a solution of the governing equations can be attained. Appendix B gives the solution for the heat-transfer coefficient when $\theta^* < \pi/2$ for two cases: (1) constant surface temperature and (b) strong surface-

temperature variation with angular position θ.

For θ^* beyond $\pi/2$ (and less than π), the similarity transform T_2 (eq. (30)) applies and a solution for the heat-transfer coefficient is presented in appendix C.

The final expressions for the heat-transfer coefficients are presented in table II.

In the expression for the heat-transfer coefficient, the effect of convection on the energy equation was neglected. Appendix G shows that the effect of convection will be of the order of 10 percent. At the expense of accuracy and for increased simplification, however, the closed-form conduction solution was used in the analysis, and λ was replaced by λ^* (eq. (G16)).

TABLE II. - SUMMARY OF SOLUTIONS TO FLOATING SPHERE PROBLEM

Transform	Boundary condition on surface temperature	Nusselt number	Constant, κ	$F(\theta^*)$	Equation number
T_2: $F_2(\zeta)(1 - \cos\theta)$, $\theta^* < \pi$	Constant at $\overline{T}_d$	$Nu_d = 1 + \left[\frac{2}{9} Ra' \left(\frac{\rho_d}{\rho_l - \rho}\right) \frac{1}{f(\theta^*)}\right]^{1/4}$ $f(\theta^*) = 1 - 2\cos\theta^* + \cos^2\theta^*$	$\left(\frac{2}{9}\right)^{1/4}$	$f(\theta^*)$	(C25a)
T_1: $F_1(\zeta)\sin^2\theta)$, $\theta^* < \pi/2$	Constant at $\overline{T}_d$	$Nu_d = 1 + \left[\frac{Ra'}{6G(\theta^*)} \left(\frac{\rho_d}{\rho_l - \rho}\right)\right]^{1/4}$ $G(\theta^*) = \frac{g(\theta^*)}{1 + \cos\theta^*}$ $= \frac{1 - \frac{3}{2}\cos\theta^* + \frac{1}{2}\cos^3\theta^*}{1 + \cos\theta^*}$	$\left(\frac{1}{6}\right)^{1/4}$	$G(\theta^*)$	(B45a)
	Strong variation with angular position θ	$Nu_d = 1 + \left[\frac{Ra'}{3g(\theta^*)} \left(\frac{\rho_d}{\rho_l - \rho}\right) \frac{\cos\theta_{ref}}{\epsilon_1}\right]^{1/4}$ where $\cos\theta_{ref}/\epsilon_1$ is some arbitrary constant, usually near 1/2	$\left(\frac{\cos\theta_{ref}}{3\epsilon_1}\right)^{1/4}$	$g(\theta^*)$	(B66a)

COMPARISON OF EXPERIMENT AND THEORY

A simple test of the analytical model is performed using water and liquid nitrogen. Liquid nitrogen represents the supporting surface, called the evaporative fluid material, shown in figure 1. When small quantities of water are placed on the surface, the water

forms a spherical drop because of the action of surface tension. At the expense of the internal energy of the water spheroid, liquid nitrogen is vaporized beneath the sphere. This vapor forms the supporting cushion for the sphere, which appears to "float" on the much colder nitrogen surface (liquid-liquid film boiling).

During the experiment, a slight amount of dye coloring was added to the water. During the freezing process, the dye color changes and continues to change until the entire drop is frozen. The frozen drop is now a hard sphere "floating" on a sea of liquid nitrogen (solid-liquid film boiling). Its free-floating state is sharply terminated at the onset of nucleate boiling, and the sphere falls beneath the surface.

The size of the water sphere used can be determined by measuring the residue (the hard sphere of ice) or by using a pipette. Both techniques were used. A stop clock was used to determine the elapsed time between placing the water on the nitrogen and the color change in the sphere, time for the sphere to be completely frozen, and the time for the sphere to fall to the bottom.

In performing the experiment, the water sphere fell about half a centimeter onto the liquid nitrogen. As film boiling must be initiated (negligible radiation) through contact of the participating elements, in this case the two fluids, a thin layer of ice could form beneath the sphere. If this hypothesis is correct, the ice layer would grow very slowly until the internal temperature of the liquid were sufficiently low, at which time the ice layer would advance quite rapidly. It seems there would be little convection, in light of the stability provided by the temperature gradient. There is, however, a natural inverse gradient at 4° C and liquid subcooling is certainly a factor. The inverse gradient could enhance the freezing rate because of the density inversion occurring at this temperature; conversely, the subcooling would degrade the freezing rate. These effects could be self-cancelling.

To use the experimentally measured sphere freezing times as a check on the theoretically determined heat-transfer coefficients, it is necessary to determine the temperature of the sphere as a function of time during freezing. Two models are used. The first, a simplified model, assumes that no thermal gradients exist in the sphere. This is analogous to the classical Newtonian cooling problem. The second model, called the pseudo-steady-state model, takes into account thermal gradients in the freezing sphere (no subcooling). The calculated time-temperature histories in the freezing sphere for both models are shown in figure 4. The derivation for the pseudo-steady-state model (lower pair of curves in fig. 4) is given in appendix I. Only the simplified model for sphere temperature is presented in the main text.

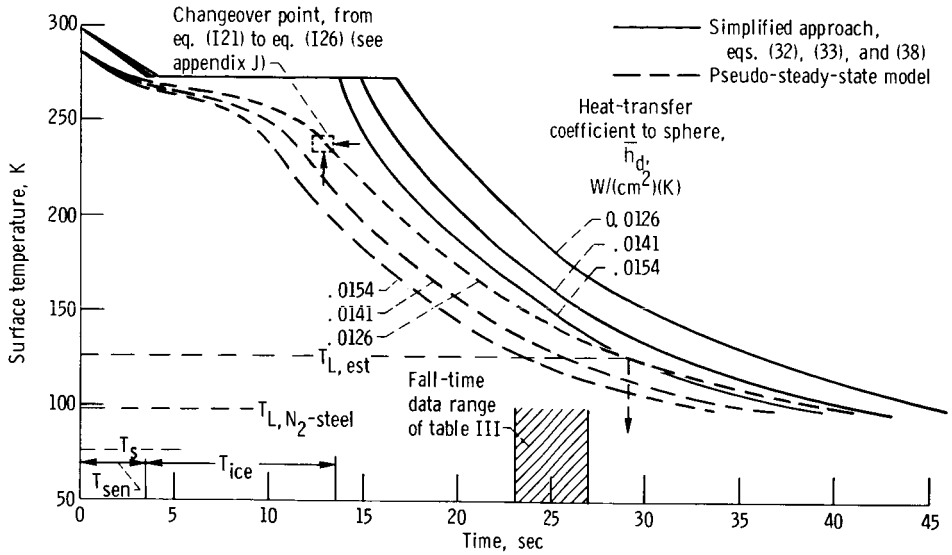

Figure 4. - Calculated surface temperature for 0.61-centimeter-diameter water sphere on liquid nitrogen as function of time.

In the simplified model calculations, the surface of the water sphere is assumed to be at 0° C and to remain at that temperature until the remainder of the sphere reaches 0° C. Therefore, neglecting the mass of the small, initial, free ice layer, the sensible cooling time can be found from an energy balance on the sphere

$$(hA)_d(T_f - T_s)t_{sen} = m\left(C_p\right)_d(T_{d,o} - T_f) \tag{31}$$

Solving for the time to remove the sensible heat t_{sen} gives

$$t_{sen} = \frac{m\left(C_p\right)_d(T_{d,o} - T_f)}{(hA)_d(T_f - T_s)} \tag{32}$$

For a 0.61-centimeter-diameter water sphere on nitrogen, the value of t_{sen} is 4.2 seconds, as shown in figure 4 (see eq. (J21), appendix J, for the numerical calculation).

The time required to freeze the entire sphere isothermally can be calculated in the same manner, only $C_p \Delta T$ is replaced by the latent heat of fusion γ, that is,

$$t_{ice} = \frac{m_{ice}\gamma}{(hA)_d(T_f - T_s)} \tag{33}$$

For the 0.61-centimeter-diameter water sphere on nitrogen, the value of t_{ice} is 12.5 seconds. This is represented by the horizontal section of the upper curves in figure 4.

Once the entire sphere has turned to ice, the solid sphere loses its sensible energy and cools to the temperature of the supporting liquid. The sensible cooling time can be found from an energy balance on the sphere, of the form

$$h_d A(T_d - T_s) = -\left(\rho C_p\right)_{ice} V \frac{\partial(T_d - T_s)}{\partial \tau} \tag{34}$$

where

$$\tau = t - (t_{sen} + t_{ice}) \tag{35}$$

and at $\tau = 0$, the surface temperature $T(0)$ is taken as the freezing temperature T_f. The solution of equation (34) becomes (for an average value of $h_d/\left(\rho C_p\right)_{ice}$),

$$\frac{T_d - T_s}{T_f - T_s} = \exp\left[-\frac{h_d A}{\left(\rho C_p\right)_{ice} V}\tau\right] \tag{36}$$

or solving for the time τ,

$$\tau = -\frac{R_o\left(\rho C_p\right)_{ice}}{3h_d} \ln\left|\frac{T_d - T_s}{T_f - T_s}\right| \tag{37}$$

Thus, the time for a sphere to freeze to some temperature beneath its freezing point is

$$t = t_{sen} + t_{ice} + \frac{R_o\left(\rho C_p\right)_{ice}}{3h_d} \ln\left|\frac{T_f - T_s}{T_d - T_s}\right| \tag{38}$$

From this equation, the temperature falloff shown by the upper curves in figure 4 is predicted.

As mentioned earlier, as the free-floating sphere cools and its outside surface temperature approaches the saturation temperature, film boiling ceases and nucleate boiling begins. At the onset of nucleate boiling, the sphere is wetted and falls beneath the surface. The transition temperature at which nucleate boiling occurs is called the Leidenfrost temperature. Assuming, for a moment, that the Leidenfrost temperature is accurately known, the important temperature in predicting the transition temperature is then the outside surface temperature of the sphere T_o. It can be shown that

$$T_o < T_d \tag{39}$$

That is, at a given time, the outside temperature of the sphere T_o will always be less than the temperature T_d calculated from the simplified analysis. This is because a temperature gradient always exists throughout the sphere. Consequently, the more exact pseudo-steady-state analysis given in appendixes I and J predicts the lower curves in figure 4. In either case, the sphere is assumed to be smooth.

The Leidenfrost temperature for water on nitrogen was estimated to be 126.0 K (see appendix K for estimation). This is illustrated by the line labeled $T_{L,est}$ in figure 4. In determining $T_{L,est}$, consideration was made for surface material and roughness (ice protrusions). The surface temperature of the 0.61-centimeter-diameter water sphere falls to this value in 29.2 seconds, at which time transition boiling begins and the sphere sinks. The theory is in reasonable agreement with the data of table III (see also fig. 4).

Additional calculations for other key times associated with the freezing of the sphere are given in appendix J.

TABLE III. - FREEZING DATA ON SMALL SPHERICAL WATER DROPS FLOATING ON LIQUID NITROGEN AT AMBIENT CONDITIONS

[Initial sphere temperature, 298 K.]

Volume of sphere, V_d, cm^3	Radius of sphere, R_o, cm	Time for dye change to become visible, sec	Time for sphere to be completely frozen, sec	Time for sphere to fall to bottom, sec
[a] 0.09	0.278	7	16	27
.113	[a] .3	8	17	23
[a] .075	.26	9	17	28
[a] .11	.295	9	18	27

[a]Measured value.

CONCLUSIONS

Theoretical expressions for the heat-transfer coefficient between a liquid sphere floating in film boiling and the supporting cryogenic fluid were derived from the fundamental equations of momentum and energy. The expression for the heat-transfer coefficient and the pseudo-steady-state freezing analysis lead to an accurate prediction of the time necessary for a sphere at room temperature to freeze when placed on the cryogenic

fluid. Further analysis of the freezing process (which is quite complex) and the use of instrumented spheres are required.

The heat-transfer coefficient to a sphere floating on the surface in film boiling is shown to be equal to

$$h_d = \frac{k}{R_o} + \kappa\left[\frac{k^3 g \rho_d \rho \lambda^*}{R_o \mu (T_d - T_s) F(\theta^*)}\right]^{1/4}$$

where k is thermal conductivity, R_o radius of sphere, κ a constant (see table II), g acceleration of local gravity, ρ_d density of sphere, ρ density of vapor, λ^* modified latent heat of vaporization, μ viscosity, T_d sphere temperature, T_s saturation temperature of liquid, $F(\theta^*)$ represents $f(\theta^*)$ or $G(\theta^*)$ for $\theta^* < \pi$ and $\theta^* < \pi/2$, respectively. These functions and nondimensional forms of the heat-transfer solution are given in table II. As seen in this equation, there are two distinct contributing factors to the heat-transfer coefficient. The first term represents the heat conduction from a sphere to a stagnant fluid, while the second term represents a contribution similar to that for parallel-surface Leidenfrost boiling.

The stagnant conduction will dominate whenever the radius of the sphere R_o is such that

$$R_o < \kappa^{4/3}\left[\frac{k\mu(T_d - T_s)}{\rho_d \rho g \lambda F(\theta^*)}\right]^{1/3}$$

Two separate and distinct transitions are seen in the film boiling of a room-temperature liquid sphere on a cryogenic surface. First, the sphere cools from room temperature and freezes. For water drops containing a blue dye, the freezing process becomes visible to the eye by a very noticeable change in the dye color. Secondly, when the sphere temperature cools into the nucleate boiling region, the supporting vapor layer is destroyed and the sphere falls beneath the surface.

Lewis Research Center,
National Aeronautics and Space Administration,
Cleveland, Ohio, January 7, 1970,
129-01.

APPENDIX A

SYMBOLS

A	surface area of sphere
$^1C, ^2C, ^3C$	constants
$C_{1,2,3,\ldots,m}$	constants
C_p	specific heat
$(C_p)_d$	specific heat of sphere
C_R	constant defined by eq. (I20)
D	differential operator
E^2	operator defined by eq. (28)
F	function defined by eq. (B2)
$F_2(\zeta)$	function defined by eq. (C2)
$F(\theta^*)$	used to represent either $f(\theta^*)$ or $G(\theta^*)$ for $\theta^* < \pi$ or $\theta^* < \pi/2$, respectively
F_σ	surface-tension force, eq. (H1)
F_b	buoyancy force, eq. (H2)
$f(\theta^*)$	function defined by eq. (C30)
$G(\theta^*)$	$g(\theta^*)/(1 + \cos \theta^*)$
Gr	Grashoff number, eq. (B69) as $\rho(\rho_l - \rho)R_o^3 g/\mu^2$
g	acceleration of local gravity
g_c	gravitational constant in Newton's law of motion
$g(\theta^*)$	function defined by eq. (D26)
h_d	heat-transfer coefficient to sphere
h_i	heat-transfer coefficient at interface
$I_{1,2,3,4}$	nondimensional components of force
$i_{1,2,3,4}$	components of force
K	index
k	thermal conductivity
L^2	characteristic length
m	mass of water sphere
m_C	arbitrary constants, $m = 1, 2, 3, \ldots$
m_{ice}	mass of ice formed
Nu_d	Nusselt number at sphere-vapor interface, $h_d R_o/k$
Nu_o	Nusselt number at surface of sphere
Nu_i	Nusselt number at vapor-liquid interface, $h_i R_o/k$
N_Φ	membrane force acting in meridian plane, fig. 9

N_θ	membrane force acting in parallel circle plane, fig. 9
P	pressure
P_o	atmospheric pressure
Pr	Prandtl number
p	dimensionless pressure, $P/(\rho u^{*2}/g_c)$
p_a	dimensionless atmospheric pressure, $P_o/(\rho u^{*2}/g_c)$
R_1, R_2	Gaussian radii of curvature
R_3	radius defined in fig. 9
Ra'	modified Rayleigh number, eq. (B70)
Re	Reynolds number, $\rho u^* R_o/\mu$
R_o	radius of sphere
r	radial coordinate
S	property group defined by eq. (B30)
T	temperature
T_d	sphere temperature
$(T_d)_{ref}$	reference temperature, eq. (F10)
T_f	film temperature, $(T_d + T_s)/2$
T_o	surface temperature during freezing, see appendix I
T_s	saturation temperature of liquid
t	time
t_{ice}	time for heat of fusion to be removed from sphere
t_{obs}	observed time for sphere to freeze
t_{sen}	time necessary for sensible heat to be removed from sphere
u*	dimensionless velocity, ν/R_o
V_d	volume of sphere
V_r	radial velocity component
V_δ	radial velocity at liquid-vapor interface
V_θ	tangential velocity component
v_ζ	dimensionless velocity in radial direction, V_r/u^*
v_Δ	velocity at interface
v_θ	dimensionless velocity in tangential direction, V_θ/u^*
W_d	weight of sphere
w*	nondimensionalizing factor, $\rho u^* R_o^2/g_c$
Y_F	surface force, fig. 9
y	dummy variable
Z	coordinate, fig. 9
Z_o	initial pressure head, fig. 8
z	dimensionless length, Z/L
β	dimensionless thickness, $1 - (r_f/R_o)$
Γ	dimensionless temperature defined by eq. (I5)
γ	latent heat of fusion
Δ	dimensionless gap thickness, δ/R_o
Δ_A	approximation for Δ, transform T_1

Δ_S similarity form for Δ, transform T_1

δ vapor-gap thickness

ϵ constant, $0 < \epsilon < 1$, fraction of temperature difference $(T_d - T_s)$

ζ dimensionless radial coordinate, r/R_o

Θ dimensionless temperature, $(T - T_d)/(T_s - T_d)$

Θ_c dimensionless temperature, $(T - T_s)\Big/\left[\left(T_d\right)_{ref} - T_s\right]$

θ angular coordinate

θ_{ref} angular position for evaluating $\left(T_d\right)_{ref}$, eq. (F8)

θ^* defined in fig. 1

κ constant, see table II

λ latent heat of vaporization

λ^* modified latent heat of vaporization, $\lambda\left\{1 + \frac{1}{2}\left[\frac{C_p(T_d - T_s)}{\lambda}\right]\right\}$

Λ convection correction term, eq. (G11)

μ viscosity

ν kinematic viscosity

ξ $1/k\rho_m C_p$

ξ_{steel} ξ evaluated for stainless-steel properties

ξ_{ice} ξ evaluated for ice properties

ρ density of vapor

ρ_d density of sphere

ρ_l density of liquid

ρ_m density of material

σ surface tension

τ dummy variable

$\tau_{r\theta}, \tau_{rr}$ shear stresses, see fig. 2

$\tau_{\zeta\theta}, \tau_{\zeta\zeta}$ dimensionless shear stresses

Φ angular coordinate defined as used, see figs. 2 and 9

φ dimensionless function, $1 + \Delta = 1 + (\delta/R_o)$

ψ stream function

Ω $W_d/\left[8\pi w^* Sg(\theta^*)\right]$

ω angular coordinate, see fig. 8

Subscripts:

A approximation for Δ

amb ambient

d sphere

f freezing

fb film boiling

ice frozen material

L Leidenfrost

l liquid

o initial

obs observed

S similarity form for Δ

s saturation

r radial direction

ref reference

tot total

v vapor

Superscripts:

$\bar{}$	average value
$'$	derivative with respect to independent variable

APPENDIX B

SOLUTION OF HEAT-TRANSFER COEFFICIENT FOR FIRST SIMILARITY TRANSFORM T_1 (WHERE $\theta^* < \pi/2$)

The momentum and energy equations were presented in the body of this report along with the final solutions. The details of the analyses are presented in this appendix.

MOMENTUM EQUATIONS

The governing momentum equations for the flow in the r and θ directions beneath the drop (see fig. 1) are given by equations (3) and (4) in the body of this report. The momentum equations were made nondimensional (eqs. (20) and (21)) and then combined into a single fourth-order equation by the use of the stream function ψ

$$E^4\psi = 0 \tag{27}$$

where

$$E^2 \equiv \frac{\partial^2}{\partial\zeta^2} + \frac{\sin\theta}{\zeta^2}\frac{\partial}{\partial\theta}\left(\frac{1}{\sin\theta}\frac{\partial}{\partial\theta}\right) \tag{28}$$

and the stream function ψ is defined in equations (23) and (24).

In order to solve equation (27), it must first be converted into a ordinary differential equation. The first of two possible similarity transforms

$$\psi_1(\zeta,\theta) = F_1(\zeta)\sin^2\theta \tag{29}$$

is used to convert equation (27) into an ordinary differential equation. Another possible similarity transform is discussed in appendix C. The transform given by equation (29) has also been used for solving the problem of flow around a sphere (ref. 7, p. 132). Substituting the similarity transform given by equation (29) into the governing equation (27) yields

$$\left(D_\zeta^2 - \frac{2}{\zeta^2}\right)\left(D_\zeta^2 - \frac{2}{\zeta^2}\right)F_1(\zeta) = 0 \tag{B1}$$

Equation (B1) is a linear fourth-order homogeneous equation, the solution of which is

$$F_1(\zeta) = \frac{C_1}{\zeta} + C_2\zeta + C_3\zeta^2 + C_4\zeta^4 \tag{B2}$$

The expressions for the dimensionless velocities v_ζ and v_θ are given in terms of the stream function ψ by equations (25) and (26) in the body of this report. Substituting equation (B2) into equations (25) and (26) gives

$$v_\zeta = \frac{-2F_1 \cos\theta}{\zeta^2} \tag{B3}$$

$$v_\theta = \frac{F_1' \sin\theta}{\zeta} \tag{B4}$$

The constants in the previous equations must be determined from the boundary conditions (eqs. (8) and (9), table I in the body of the report; note that eq. (10) is satisfied by (B4)). In terms of the dimensionless variables, these boundary conditions become

$$v_\theta(1, \theta) = 0 \tag{B5}$$

$$v_\theta(1 + \Delta, \theta) = 0 \tag{B6}$$

$$v_\zeta(1, \theta) = 0 \tag{B7}$$

$$v_\zeta(1 + \Delta, \theta) = v_\Delta \tag{B8}$$

where

$$\Delta \equiv \frac{\delta}{R_o} \tag{B9}$$

Here, Δ represents the dimensionless vapor-gap thickness concentric with the sphere.

Applying these conditions allows the four constants to be expressed in terms of one constant of integration, as follows:

$$C_1 = -\frac{2C_4}{1 + \varphi + 4\varphi^2}\left[-\varphi^2 + 2\varphi^3 + 2\varphi^4\right] \tag{B10}$$

$$C_2 = \frac{2C_4}{1 + \varphi + 4\varphi^2}\left[1 + \varphi + \varphi^2 + 6(\varphi^3 + \varphi^4)\right] \tag{B11}$$

$$C_3 = -\frac{C_4}{1 + \varphi + 4\varphi^2}\left[3 + 3\varphi + 8(\varphi^2 + \varphi^3 + \varphi^4)\right] \tag{B12}$$

where

$$\varphi = 1 + \Delta \tag{B13}$$

The dimensionless gap thickness Δ is assumed at this time to be an unknown constant. However, as is shown later (e.g., see eq. (B27)), this requires that the interface energy balance be satisfied on an average over the heating surface, rather than at every point.

The constant C_4 can be found by applying the static force balance constraint (eq. (12)). First, however, the pressure distribution in the vapor gap must be expressed in terms of the unknown constants. Substituting equations (B3) and (B4) into equations (20) and (21) and solving for the pressure distribution give

$$p(\zeta,\theta) = -\cos\theta\left(F_1''' + \frac{4F_1}{\zeta^3} - \frac{2F_1'}{\zeta^2}\right) + {}^3C \tag{B14}$$

which upon substituting in the value of F_1 gives

$$p(\zeta,\theta) = -\cos\theta\left(20C_4\zeta + \frac{2C_2}{\zeta^2}\right) + {}^3C \tag{B15}$$

where C_2 is related to C_4 by equation (B11).

Now, the constants C_4 and ${}^3C$ are determined from the static force balance in appendix D. This gives

$$C_4 = -\left(\frac{W_d}{8\pi w^*}\right)\frac{1 + \varphi + 4\varphi^2}{\left[1 + \varphi + \varphi^2 + 6(\varphi^3 + \varphi^4)\right]g(\theta^*)} \tag{B16}$$

where

$$g(\theta^*) = 1 - \frac{3}{2}\cos\theta^* + \frac{1}{2}\cos^3\theta^* \tag{D26}$$

and

$$^3C = p_a + \cos\theta^*\,(20C_4 + 2C_2) \tag{B17}$$

where w^* is defined by equation (B25) as $w^* = \rho u^{*2} R_o^2/g_c$.

Therefore, utilizing C_4 in C_1, C_2, and C_3, the velocity and pressure distributions are known relations in φ where $\varphi = 1 + \Delta$.

The energy equation is considered in the next section. Afterwards, the solutions to the energy and momentum equations are combined in the interface energy balance to obtain a solution for the heat-transfer coefficient.

ENERGY EQUATION

The energy equation is solved in appendix F for both constant surface temperature $T = T_d$ at $r = R_o$ (eq. (8), $\epsilon = 0$) and for a strong circumferential variation in surface temperature $T = T_d + \epsilon(T_d - T_s)\cos\theta$ at $r = R_o$ (eq. (8)). Consider first the constant temperature solution ($\epsilon = 0$) in detail, then the θ-dependent solution.

Constant Surface Temperature, $T = T_d$

The nondimensional form of the energy equation (eq. (6)) becomes

$$\frac{\partial}{\partial\zeta}\left(\zeta^2\frac{\partial\Theta}{\partial\zeta}\right) = 0 \tag{B18}$$

where

$$\Theta = \frac{T - T_d}{T_s - T_d} \tag{B19}$$

which can be solved directly. From appendix F the solution is

$$\Theta = \frac{\varphi}{\Delta}\left(1 - \frac{1}{\zeta}\right) \tag{B20}$$

The temperature gradient at each surface becomes

$$\left.\frac{d\Theta}{d\zeta}\right|_{\zeta=1} = \frac{\varphi}{\Delta} \tag{B21}$$

$$\left.\frac{d\Theta}{d\zeta}\right|_{\zeta=1+\Delta} = \frac{1}{\varphi\Delta} \tag{B22}$$

Interface energy balance. - The velocity and temperature distributions have been expressed up to this point in terms of an unknown parameter, the dimensionless vapor-gap thickness Δ. The interface energy balance (eq. (13)) is now used to determine the value of this parameter.

First, the radial velocity at the interface must be determined. Substituting the values of the constants C_1 to C_4 (eqs. (B10) to (B12), and (B16)) into equation (B3) and evaluating the velocity at the interface ($\zeta = 1 + \Delta$) gives

$$v_\Delta = -\left(\frac{15W_d}{4\pi w^*}\right)\left\{\frac{1 + \Delta + \frac{4}{15}\Delta^2}{\varphi\left[1 + \varphi + \varphi^2 + 6(\varphi^3 + \varphi^4)\right]}\right\}\frac{\Delta^3 \cos\theta}{g(\theta^*)} \tag{B23}$$

For very small values of Δ, v_Δ may be approximated by

$$v_{\Delta<<1} \simeq -\left(\frac{W_d}{4\pi w^*}\right)\frac{\Delta^3 \cos\theta}{g(\theta^*)} \tag{B24}$$

where

$$w^* = \frac{\rho u^{*2} R_o^2}{g_c} \tag{B25}$$

Substituting the expression for v_Δ (eq. (B23)) into the interface energy balance (the nondimensional form of eq. (13)), imposing the constant-temperature boundary constraints, and solving for Δ give

$$\Delta = f(\theta) \tag{B26}$$

This gives rise to a serious problem in the mathematical operation at this time, since

Δ is not independent of θ. Consequently, the similarity solution for this transform does not exist in terms of the variable $\psi(\zeta, \theta)$ for the constant-temperature case, since Δ had been assumed a constant in the solution of the momentum equations. However, the constant-temperature case is of great interest, and the concept of similarity conditioning is now introduced to attain a solution. This problem does not occur in the second case where surface temperature varies as $\cos \theta$, as is discussed later in this appendix.

Similarity conditioning. - From a practical engineering point of view, the answer to the similarity dilemma posed herein was to reduce the severity of the auxiliary constants given by equation (13). As in many analyses, simplifications are made to the physics and then checked for validity. Thus, instead of requiring the interface energy balance to hold at every point on the boundary, as required in equation (13), an integral boundary constraint of the following form is used in place of equation (13):

$$-\rho\lambda\overline{V}_r(R_o + \delta) = -k \left.\frac{\partial T}{\partial r}\right|_{r=R_o+\delta} \tag{B27}$$

where

$$\overline{V}_r(R_o + \delta) = \frac{\displaystyle\int_0^{2\pi}\int_0^{\theta^*} \left[V(R_o + \delta)\right](R_o + \delta)^2 \sin\theta \, d\theta \, d\Phi}{\displaystyle\int_0^{2\pi}\int_0^{\theta^*} (R_o + \delta)^2 \sin\theta \, d\theta \, d\Phi} \tag{B28}$$

Here, $\overline{V}_r$ represents an average radial velocity in the vapor gap. This integral constraint conditions the problem such that a similarity transformation exists.

Similarity solution by integral boundary constraint: Nondimensionalizing equation (B27) results in the averaged energy balance

$$-\overline{v}_\Delta = S \left.\frac{d\Theta}{d\zeta}\right|_{\zeta=1+\Delta} \tag{B29}$$

where

$$S = \frac{1}{Pr}\left[\frac{C_p(T_d - T_s)}{\lambda}\right] \tag{B30}$$

At this point, Δ is an unknown function of θ. If v_Δ were constant, Δ would be independent of θ. In seeking an average value for v_Δ independent of θ, Δ, while still

an unknown, would also be independent of θ. Therefore, assuming Δ as some average value and substituting the expression for v_Δ (eq. (B23)) into the nondimensional forms of equation (B28), $\bar{v}_\Delta$ becomes

$$-\bar{v}_\Delta = \left(\frac{15W_d\Delta^3}{8\pi w^*}\right)\left[\frac{\left(1 + \Delta + \frac{4}{15}\Delta^2\right)(1 + \cos\theta^*)}{15\varphi\left(1 + 3\Delta + \frac{11}{3}\Delta^2 + 2\Delta^3 + \frac{2}{5}\Delta^4\right)g(\theta^*)}\right] \tag{B31}$$

Substituting equation (B31) into equation (B29) along with the expression for the gradient (eq. (B22)) and solving for Δ gives

$$\Delta^4 = \left(\frac{8\pi w^* S}{W_d}\right)\left[\frac{\left(1 + 3\Delta + \frac{11}{3}\Delta^2 + 2\Delta^3 + \frac{2}{5}\Delta^4\right)g(\theta^*)}{\left(1 + \Delta + \frac{4}{15}\Delta^2\right)(1 + \cos\theta^*)}\right] \tag{B32}$$

For $\Delta << 1$ and $G(\theta^*) \equiv g(\theta^*)/(1 + \cos\theta^*)$, equation (B32) becomes

$$\Delta_S = \left[\frac{8\pi w^* S G(\theta^*)}{W_d}\right]^{1/4} \tag{B33}$$

Thus, Δ is independent of ζ and θ, but dependent on θ^*, and the similarity solution exists.

Approximate solution for small angular displacements: As discussed previously, some of the natural physics of the problem were relaxed in order to preserve similarity and obtain a separable solution to the differential system.

In this section, it is shown that, given a value of angular position θ, similarity will be approximately preserved for small angular displacements. This requires that C_1 to C_4 be independent of angular displacement. The constant C_2 is already an absolute constant, as is now shown. Substituting the value of C_4 (eq. (B16)) into the expression for C_2, equation (B11) gives

$$C_2 = -\left[\frac{W_d}{4\pi w^* g(\theta^*)}\right] \tag{B34}$$

Thus, the constants C_1, C_3, and C_4 need only be examined in detail to determine their dependence on ζ and θ. The variation of F_1 (eq. (B2)) can then be determined.

The interface energy balance (eq. (13)) without the integral constraint can be written as

$$-v_{\Delta} = S \left.\frac{d\Theta}{d\zeta}\right|_{\zeta=1+\Delta} \tag{B35}$$

which is similar to equation (B29) except there is no bar to indicate an average quantity.

Substituting the value for v_{Δ} (eq. (B23)) and the expression for the temperature gradient (eq. (B22)) into equation (B35) and rearranging terms give

$$\Delta^4 = \frac{-(1 + \varphi + 4\varphi^2)S}{30 \cos \theta \left(1 + \Delta + \frac{4}{15}\Delta^2\right) C_4} \tag{B36}$$

Substituting into equation (B36) the value of C_4 from equation (B16) gives

$$\Delta^4 = \frac{4\pi w^* S}{W_d \cos \theta} \left(\frac{1 + 3\Delta + \frac{11}{3}\Delta^2 + 2\Delta^3 + \frac{2}{5}\Delta^4}{1 + \Delta + \frac{4}{15}\Delta^2} \right) g(\theta^*) \tag{B37}$$

For small Δ, a first approximation for equation (B37) is

$$\Delta_A = \left[\frac{4\pi w^* S g(\theta^*)}{W_d \cos \theta} \right]^{1/4} \tag{B38}$$

As θ approaches $\pi/2$ (which implies that $\theta^* \to \pi/2$), Δ_A becomes very much greater than 1.

Since C_1, C_3, and C_4 are functions of Δ (see eqs. (B10) to (B13), and (B16)), they turn out to be pseudoconstants which are constrained by sec θ. However, the solution to the differential system was based on a separable solution. The constants C_1, C_3, and C_4 being functions of θ clearly violate this premise. Nevertheless, approximate similarity would be preserved, if for small angular displacements the constants were indeed invariant. The variation with angular position in the pseudoconstants, the gap thickness Δ_A, the interface velocity v_{Δ}, and the pseudofunction F_1 is presented in figure 5, using the approximate solution for Δ.

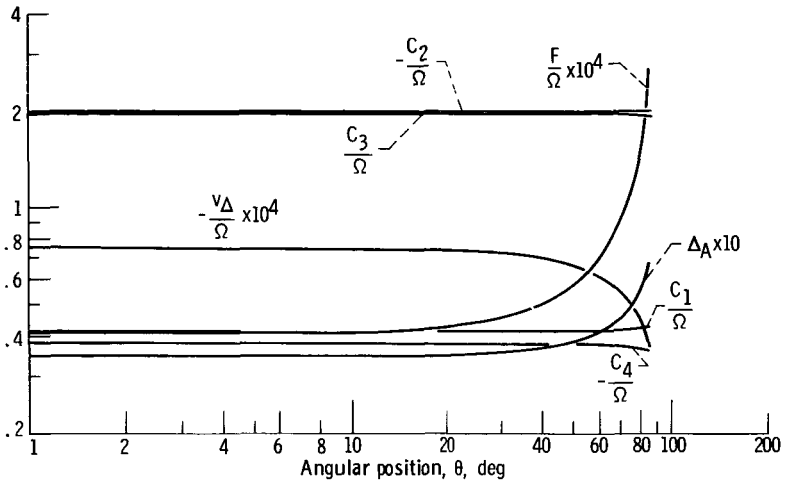

Figure 5. - Variation of gap thickness Δ, interface velocity v_Δ, and pseudo-steady-state parameters with angular position ($\theta^* \rightarrow \pi/2$, $\zeta = \varphi$, and $\Omega = 3.55 \times 10^5$).

As seen in figure 5, for $\theta < 30^\circ$ the pseudoconstants C_1, C_3, and C_4 are very nearly constant; however, Δ_A, v_Δ, and F vary 3, 4, and 10 percent, respectively. For $\theta < 86^\circ$, they vary as follows:

$$C_1 < 4 \text{ percent}; \quad C_3 < 3 \text{ percent}; \quad C_4 < 8 \text{ percent} \tag{B39}$$

However, as evident from figure 5, F changes by a factor of 6.65, which is clearly a violation of the separability hypothesis. Nevertheless, the pseudo-solution points out that as Δ_A increases, v_Δ decreases; this means that the heat transfer at the interface is decreasing, which is in agreement with reality. These errors at small angles are quite acceptable considering the physical intuition gained by this approximate technique; however, at large angles, the error in F is considerable, and the results are highly questionable.

The values of Δ_A and Δ_S in equations (B33) and (B38) differ only by a factor

$$\left(\frac{2 \cos \theta}{1 + \cos \theta^*}\right)^{1/4} \tag{B40}$$

However, at θ equal to 60^o and assuming $\theta^* \to \pi/2$, both the similarity and approximate solutions for Δ agree. This implies that both solutions can be made to agree in an average sense, which, in turn, implies the surface-averaged heat-transfer coefficients are about the same

$$h_A \approx h_S \tag{B41}$$

Heat-transfer coefficient. - The heat-transfer coefficient can now be constructed from the momentum and energy solutions. Because the approximate and similarity solutions presented in the last section differ only by a constant when average values are considered, only the similarity case is considered here.

Sphere surface: The heat-transfer coefficient to the sphere is defined as

$$h_d(T_d - T_s) = -k \left.\frac{\partial T}{\partial r}\right|_{r=R_o} \tag{B42}$$

Utilizing the nondimensional forms, h_d can be written as

$$\frac{h_d R_o}{k} = \left.\frac{\partial \Theta}{\partial \zeta}\right|_{\zeta=1} \tag{B43}$$

Substituting equation (B21) into equation (B43) gives

$$\frac{h_d R_o}{k} = 1 + \frac{1}{\Delta} \tag{B44}$$

Substituting the expression for Δ given by equation (B33) into equation (B44) gives

$$\underbrace{Nu_d = \frac{h_d R_o}{k}}_{\text{Nusselt number for sphere}} = \underbrace{1}_{\substack{\text{Heat conduction from sphere to stagnant fluid}}} + \underbrace{\left[\frac{W_d}{8\pi w^* SG(\theta^*)}\right]^{1/4}}_{\substack{\text{Concentric-surface Leidenfrost phenomenon contribution}}} \tag{B45}$$

In dimensional form, the gap thickness can be expressed as

$$\delta = R_o \Delta = R_o \left[\frac{8\pi\nu k(T_d - T_s)G(\theta^*)}{\rho_d V_d g\lambda}\right]^{1/4} \tag{B46}$$

This was accomplished by substituting the dimensional forms of S (eq. (B30)) and w^* (eq. (B25)) into equation (B33). In a similar manner, the heat-transfer coefficient may be written

$$h_d = \frac{k}{R_o} + \left[\frac{\rho_d V_d g\lambda^* k^3}{8\pi R_o^4 \nu(T_d - T_s)G(\theta^*)}\right]^{1/4} \tag{B47}$$

where λ has been replaced by λ^* to compensate for convection effects, see appendix G. But

$$V_d = \frac{4}{3}\pi R_o^3 \tag{B48}$$

therefore,

$$h_d = \frac{k}{R_o} + 0.64\left[\frac{k^3 \rho_d \rho g\lambda^*}{R_o \mu(T_d - T_s)G(\theta^*)}\right]^{1/4} \tag{B49}$$

This equation indicates that the stagnant conduction term k/R_o will begin to dominate whenever the radius of the sphere is such that

$$\frac{k}{R_o} \simeq 0.64\left[\frac{k^3\rho_d\rho g\lambda^*}{R_o\mu(T_d - T_s)G(\theta^*)}\right]^{1/4} \tag{B50}$$

or

$$R_o < 1.81\left[\frac{k\mu(T_d - T_s)G(\theta^*)}{\rho_d\rho g\lambda^*}\right]^{1/3} \tag{B51}$$

That is, when the gap thickness becomes larger than the sphere radius, stagnant conduction would dominate; and, of course, the entire solution becomes questionable.

If at this point the similarity solution is compared to the approximate solution (refer back to section Interface energy balance), the approximate solution indicates that as θ approaches $\pi/2$ (which implies $\theta^* \to \pi/2$),

$$h_d = \frac{k}{R_o} \qquad \text{for} \quad \theta \to \pi/2 \tag{B52}$$

That is, the heat-transfer coefficient returns to the stagnant flow contribution of a sphere in an infinite media.

Liquid interface: The heat transfer at the interface between the vapor and the supporting liquid is given by

$$h_i(T_d - T_s) = -k\left.\frac{\partial T}{\partial r}\right|_{r=R_o+\delta} \tag{B53}$$

Nondimensionalizing this equation and substituting equation (B22) into the result yield

$$\frac{h_i R_o}{k} = \frac{1}{\Delta(1 + \Delta)} \simeq \frac{1}{\Delta} - 1 \tag{B54}$$

Substituting the value for Δ given by equation (B33) into equation (B47) gives

$$Nu_i = \frac{h_i R_o}{k} = \left[\frac{W_d}{8\pi w^* SG(\theta^*)}\right]^{1/4} - 1 \tag{B55}$$

In this case, in comparison to equation (B45), the Nusselt number equals the concentric-surface Leidenfrost phenomenon contribution less that of the axisymmetric stagnation flow.

The approximation solution (refer back to section Interface energy balance), however, shows that as θ^* approaches $\pi/2$, Δ becomes large, and the approximation used in equation (B54) is no longer valid. The value of h_i is zero at this point. Conceptually, at θ^* equal to $\pi/2$, the sphere is emitting energy to an infinite stagnant region; that is,

$$h_d = \frac{k}{R_o} \qquad \text{for } \theta^* \to \frac{\pi}{2} \tag{B56}$$

while the energy never reaches the supporting interface at infinity; that is,

$$h_i = 0 \qquad \text{for } \theta^* \to \frac{\pi}{2} \tag{B57}$$

This implies that there can be no evaporation at the liquid interface at $\theta = \pi/2$ because of the presence of the drop.

Strong Surface-Temperature Variation

The second problem is that of a surface temperature variation of the form

$$T = T_d + \epsilon(T_d - T_s)\cos\theta \qquad \text{at } r = R_o \tag{8}$$

The energy equation for a strong surface-temperature variation with angular position is solved in appendix F. The solution is

$$\left.\frac{\partial \Theta_c}{\partial \zeta}\right|_{\zeta=1} = -\frac{\epsilon_1 \cos\theta}{(\varphi^3 - 1)\cos\theta_{ref}}(1 + 2\varphi^3) \tag{B58}$$

where

$$\left.\frac{\partial \Theta_c}{\partial \zeta}\right|_{\zeta=1+\Delta} = -\frac{3\epsilon_1 \cos\theta}{(\varphi^3 - 1)\cos\theta_{ref}} \tag{B59}$$

and ϵ_1 is an arbitrary positive constant (i.e., $\epsilon_1 > 0$).

The temperature gradient at each surface becomes

$$\Theta_c = -\frac{\epsilon_1}{\varphi^3 - 1}\left(\zeta - \frac{\varphi^3}{\zeta^2}\right)\frac{\cos\theta}{\cos\theta_{ref}} \qquad \text{for} \quad \theta^* < \frac{\pi}{2} \tag{F12}$$

where Θ_c is defined

$$\Theta_c = \frac{T - T_s}{(T_d)_{ref} - T_s} \tag{F10}$$

Interface energy balance. - The velocity and temperature distributions are expressed in terms of the dimensionless vapor-gap thickness Δ, and again the interface energy balance is used to determine Δ.

The radial velocity at the interface (eq. (B23)) and the temperature gradient at the interface (eq. (B59)) are substituted into the interface energy balance equation (eq. (B35))

$$-v_\Delta = S\left.\frac{d\Theta}{d\zeta}\right|_{\zeta=1+\Delta} \tag{B35}$$

$$-\left(\frac{15W_d\Delta^3}{4\pi w^*}\right)\frac{\left(1 + \Delta + \frac{4}{15}\Delta^2\right)\left[\frac{\cos\theta}{g(\theta^*)}\right]}{15\varphi\left(1 + 3\Delta + \frac{11}{3}\Delta^2 + 2\Delta^3 + \frac{2}{5}\Delta^4\right)} = -\frac{3S\epsilon_1\cos\theta}{(\varphi^3 - 1)\cos\theta_{ref}} \tag{B60}$$

where

$$g(\theta^*) \equiv 1 - \frac{3}{2}\cos\theta^* + \frac{1}{2}\cos^3\theta^* \tag{D26}$$

Solving equation (B60) for Δ gives

$$\Delta^4 = \left(\frac{4\pi w^* S\epsilon_1}{W_d\cos\theta_{ref}}\right)\varphi\,\frac{1 + 3\Delta + \frac{11}{3}\Delta^2 + 2\Delta^3 + \frac{2}{5}\Delta^4}{\left(1 + \Delta + \frac{4}{15}\Delta^2\right)\left(1 + \Delta + \frac{\Delta^2}{3}\right)}\,g(\theta^*) \tag{B61}$$

Now for $\Delta << 1$, equation (B61) reduces to

$$\Delta^4 = \frac{4\pi w^* S \epsilon_1 g(\theta^*)}{W_d \cos \theta_{ref}} \tag{B62}$$

The similarity of equations (B62), (B33), and (B38) is striking; for example, if $\epsilon_1 \to 1$ $\theta_{ref} \to \pi/3$ and $\theta \to \pi/3$, where $\theta^* \to \pi/2$, they are the same.

Heat-transfer coefficient. - As in the constant-surface-temperature case, the heat-transfer coefficient can be constructed from the momentum and energy equations.

Sphere surface: The heat-transfer coefficient to the sphere is defined as

$$h_d(T_d - T_s) = -k \left.\frac{\partial T}{\partial r}\right|_{r=R_o} \tag{B63}$$

or writing equation (B63) in nondimensional terms,

$$\frac{h_d R_o}{k} = - \frac{1}{\Theta_c\big|_{\zeta=1}} \left.\frac{\partial \Theta_c}{\partial \zeta}\right|_{\zeta=1} \tag{B64}$$

Evaluating equations (F12) and (B58) at $\zeta = 1$ and substituting into equation (B64) gives

$$\frac{h_d R_o}{k} = \frac{1 + 2\varphi^3}{\varphi^3 - 1} \tag{B65}$$

Assuming $\Delta << 1$ and substituting for Δ (eq. (63)) in the result, equation (B65) becomes

$$\frac{h_d R_o}{k} \approx 1 + \frac{1}{\Delta} = 1 + \left[\frac{W_d \cos \theta_{ref}}{4\pi w^* S \epsilon_1 g(\theta^*)}\right]^{1/4} \tag{B66}$$

If $\theta_{ref} = 60^o$ and $\epsilon_1 \to 1$, where $\theta^* \to \pi/2$, equation (B66) gives the same Nusselt number as for the constant-surface-temperature solution (eq. (B45)).

Liquid interface: The heat-transfer coefficient at the interface is given by

$$h_i = - \frac{k}{R_o \Theta_c \Big|_{\zeta=1}} \frac{\partial \Theta_c}{\partial \zeta} \Bigg|_{\zeta=\varphi} \tag{B67}$$

Substituting equations (B59) and (F12) into equation (B67) gives

$$\frac{h_i R_o}{k} = \frac{3}{\varphi^3 - 1} \approx \frac{1}{\Delta} - 1 \tag{B68}$$

Equations (B68) and (B54) are identical.

The equivalence of equation (B66) to (B45) and of equation (B68) to (B54) indicate that, insofar as heat transfer is concerned, the assumption of a constant-temperature surface with a constant vapor-gap thickness is compatible with a strong θ-temperature variation with variable gap thickness.

NONDIMENSIONAL FORMS

It is most instructive to investigate the heat-transfer-coefficient expressions for nondimensional parameters. The nondimensional forms identify the major, or first-order, terms influencing the solution. In equations (B45) and (B66), the term W_d/w^*S appears, which can be expressed as

$$\frac{W_d}{w^*S} = \frac{\frac{4}{3} \pi \rho_d R_o^3 \frac{g}{g_c}}{\frac{\rho \mu^2 R_o^2}{R_o^2 \rho^2 g_c} \frac{1}{Pr} \frac{C_p \Delta T}{\lambda}} = \frac{4\pi}{3} \left\{ \left(\frac{\rho_d}{\rho_l - \rho} \right) \left[\frac{\rho(\rho_l - \rho) R_o^3 g}{\mu^2} \right] \left(Pr \frac{\lambda}{C_p \Delta T} \right) \right\} \tag{B69}$$

The latter part of equation (B69) is the familiar Grashoff number - Prandtl number product (or Rayleigh number modified by the ratio of latent to sensible heats), and λ is replaced by λ^*

$$Ra' \equiv Ra \frac{\lambda^*}{C_p \Delta T} = GrPr \frac{\lambda^*}{C_p \Delta T} \tag{B70}$$

Substituting equations (B69) and (B70) into equations (B45) and (B66) gives

$$Nu_d = 1 + \left[\frac{Ra'}{6G(\theta^*)}\left(\frac{\rho_d}{\rho_l - \rho}\right)\right]^{1/4} \tag{B45a}$$

$$Nu_d = 1 + \left[\frac{Ra'}{3g(\theta^*)}\left(\frac{\rho_d}{\rho_l - \rho}\right)\frac{\cos\theta_{ref}}{\epsilon_1}\right]^{1/4} \tag{B66a}$$

Equations (B45a) and (B66a) indicate that Nusselt number is governed by the usual film-boiling relation $(Ra')^{1/4}$, the interrelation between density differences, and θ^*.

APPENDIX C

SOLUTION OF HEAT-TRANSFER COEFFICIENT FOR SECOND SIMILARITY TRANSFORM T_2 (WHERE $\theta^* < \pi$)

MOMENTUM EQUATION

The second similarity transform

$$\psi_2(\zeta, \theta) = F_2(\zeta)(1 - \cos \theta) \tag{30}$$

is used to convert equation (27) into an ordinary differential equation. This transformation has also been used for solving for flow around a sphere. Substituting equation (30) into equation (27) yields

$$F_2^4(\zeta) = 0 \tag{C1}$$

This is a linear homogeneous equation of fourth order which has a solution

$$F_2(\zeta) = C_1 + C_2\zeta + C_3\zeta^2 + C_4\zeta^3 \tag{C2}$$

Therefore,

$$v_\zeta = -\frac{F_2(\zeta)}{\zeta^2} \tag{C3}$$

$$v_\theta = \frac{F_2'(\zeta)\tan\frac{\theta}{2}}{\zeta} \tag{C4}$$

The constants in the previous equation must be determined from the boundary conditions (eqs. (8) and (9)). In terms of the dimensionless variables, these boundary conditions become

$$v_\theta(1, \theta) = 0 \tag{C5}$$

$$v_\theta(1 + \Delta, \theta) = 0 \tag{C6}$$

$$v_\zeta(1, \theta) = 0 \tag{C7}$$

$$v_\zeta(1 + \Delta, \theta) = v_\Delta \tag{C8}$$

where

$$\Delta \equiv \frac{\delta}{R_o} \tag{C9}$$

Applying these conditions to equations (C3) and (C4) allows the four constants to be expressed in terms of one constant of integration

$$C_1 = \frac{C_4}{2}(1 - 3\varphi) \tag{C10}$$

$$C_2 = 3C_4\varphi \tag{C11}$$

$$C_3 = -\frac{3C_4}{2}(1 + \varphi) \tag{C12}$$

where

$$\varphi = 1 + \Delta \tag{C13}$$

The dimensionless gap thickness Δ is assumed at this time to be an unknown constant. However, as shown in appendix B (eq. (B27)), this requires that the interface energy balance be satisfied on an average over the heating surface rather than at every point.

The constant C_4 can be found by satisfying the static force balance constraint. First, however, the pressure distribution in the vapor gap must be found. Substituting equations (C3) and C4) into equations (20) and (21) and solving for the pressure distribution give

$$\frac{p(\zeta, \theta)}{C_4} = \frac{-3(1 + \varphi)}{\zeta} - 6 \ln \zeta + 12 \ln\left(\sec \frac{\theta}{2}\right) + \frac{^3C}{C_4} \tag{C14}$$

The constants C_4 and ^3C are determined from the static force balance in appendix E. This gives

$$C_4 = - \frac{\frac{W_d}{3\pi w^*}}{\cos^2\theta^* - 2\cos\theta^* + 1} \tag{C15}$$

$$\frac{{}^3C}{C_4} = \frac{p_a}{C_4} + 3(1 + \varphi) - 12 \ln\left(\sec\frac{\theta^*}{2}\right) \tag{C16}$$

Therefore, utilizing C_1, C_2, C_3, and C_4, the velocity and pressure distributions are known functions of φ, where $\varphi = 1 + \Delta$.

Next, the energy equations are considered. Afterwards, the solution to the energy and momentum equations are combined in the interface energy balance to obtain a solution for the heat-transfer coefficient.

ENERGY EQUATION

The energy equation is solved in appendix F, and the general solution for a cosine variation in surface temperature of an arbitrary amplitude is (eq. (F5))

$$\Theta = \frac{\varphi}{\Delta}\left(1 - \frac{1}{\zeta}\right) + \frac{\epsilon}{\varphi^3 - 1}\left(\zeta - \frac{\varphi^3}{\zeta^2}\right)\cos\theta \tag{C17}$$

where

$$\Theta = \frac{T - T_d}{T_s - T_d} \tag{C18}$$

The temperature gradient at each surface becomes

$$\left.\frac{\partial\Theta}{\partial\zeta}\right|_{\zeta=1} = \frac{\varphi}{\Delta}(1 + \epsilon\cos\theta) \tag{C19}$$

$$\left.\frac{\partial\Theta}{\partial\zeta}\right|_{\zeta=\varphi} = \frac{1}{\Delta\varphi}\left(1 + \frac{\epsilon\cos\theta}{1 + \frac{\Delta^2}{3\varphi}}\right) \tag{C20}$$

which for small values of ϵ reduce to equations (B21) and (B22), respectively. Also note that where $\epsilon \cos \theta >> 1$, which corresponds to the strong-variation case and $\theta^* < \pi/2$, equations (C19) and (C20) are similar to equations (B58) and (B59), respectively.

INTERFACE ENERGY BALANCE

The velocity and temperature distributions are expressed in terms of two unknowns, Δ and θ^*. The interface energy balance is used to determine Δ in terms of θ^*.

Substituting the values of constants C_1 to C_3 into equation (C3) and evaluating v_ζ at φ give the interface velocity

$$\frac{v_\Delta}{C_4} = -\frac{1}{2}\left(\frac{1 - 3\varphi}{\varphi^2} + 3 - \varphi\right) \tag{C21}$$

where C_4 is a function of θ^* and the parameter W_d/w^* (see eq. (C15)).

Nondimensionalizing equation (13), the interface energy balance becomes

$$v_\Delta = -S \left.\frac{\partial \Theta}{\partial \zeta}\right|_{\zeta=\varphi} \tag{C22}$$

where

$$S = \frac{1}{Pr}\left[\frac{C_p(T_d - T_s)}{\lambda^*}\right] \tag{B29}$$

and λ has been replaced by λ^* to accommodate some effects of convection (see appendix G).

Substituting equations (C15) and (C21) into (C22) gives, for $\varphi \approx 1$,

$$\Delta^4 = \left(\frac{6\pi w^* S}{W_d}\right)(\cos^2\theta^* - 2\cos\theta^* + 1)\left(1 + \frac{\epsilon \cos\theta}{1 + \frac{\Delta^2}{3}}\right) \tag{C23}$$

The problem here is, as in appendix B, the value of θ^* and how to assign $\epsilon \cos \theta$ so as to maintain similarity. The latter is solved by assigning

$$\epsilon = 0 \tag{C24}$$

The value of θ^* is determined from the balance of forces at the interface (see appendix H).

HEAT-TRANSFER COEFFICIENT

Sphere Surface

The Nusselt number for the sphere is given by

$$\frac{h_d R_o}{k} = \left.\frac{\partial \Theta}{\partial \zeta}\right|_{\zeta=1} \tag{B43}$$

Substituting equations (C19), (C23), and (C24) into equation (B43) gives (assuming $\Delta \ll 1$)

$$\frac{h_d R_o}{k} = 1 + \left[\frac{W_d}{6\pi w^* S(\cos^2\theta^* - 2\cos\theta^* + 1)}\right]^{1/4} \tag{C25}$$

where θ^* is determined in appendix H.

Liquid Interface

The nondimensional form of equation (B53) gives the Nusselt number at the interface

$$\frac{h_i R_o}{k} = \left.\frac{\partial \Theta}{\partial \zeta}\right|_{\zeta=\varphi} \tag{C26}$$

Substituting equations (C20), (C23), and (C24) into (C26) gives

$$\frac{h_i R_o}{k} = \frac{1}{\Delta\varphi} \approx -1 + \frac{1}{\Delta} \tag{C27}$$

$$\frac{h_i R_o}{k} = -1 + \left[\frac{W_d}{3\pi w^* S(\cos^2\theta^* - 2\cos\theta^* + 1)}\right]^{1/4} \tag{C28}$$

where, again, θ^* is determined in appendix H.

NONDIMENSIONAL FORMS

In appendix B the basic nondimensional terms governing the solution were identified; these parameters and W_d/w^*S are given by equations (B69) and (B70) as

$$\frac{W_d}{w^*S} = \frac{4\pi}{3} Ra' \frac{\rho_d}{\rho_l - \rho} \tag{C29}$$

Substituting equation (C29) into equations (C28) and (C25) indicates that heat transfer is influenced by the usual $Ra'^{1/4}$ and the interrelation between the density ratio $\rho_d/(\rho_l - \rho)$ and θ^*, as was shown in appendix B.

$$\frac{h_d R_o}{k} = 1 + \left[\frac{4}{9} Ra' \left(\frac{\rho_d}{\rho_l - \rho}\right) \frac{1}{f(\theta^*)}\right]^{1/4} \tag{C25a}$$

$$\frac{h_i R_o}{k} = -1 + \left[\frac{4}{9} Ra' \left(\frac{\rho_d}{\rho_l - \rho}\right) \frac{1}{f(\theta^*)}\right]^{1/4} \tag{C28a}$$

where

$$f(\theta^*) = \cos^2\theta^* - 2\cos\theta^* + 1 \tag{C30}$$

APPENDIX D

STATIC FORCE BALANCE FOR TRANSFORMATION T_1 (WHERE $\theta^* < \pi/2$)

The pressure distribution beneath the spherical drop comes directly from the solution of the momentum equations and is given by equation (B15) (repeated here for convenience) as

$$p(\zeta, \theta) = -\cos\ \theta\left(20C_4\zeta + \frac{2C_2}{\zeta^2}\right) + {}^3C \tag{B15}$$

where C_4 and C_2 are related by equation (B11). The purpose of this appendix is the determination of the two unknown constants C_4 and ${}^3C$ by the application of boundary condition equation (11) and the static force balance given by equation (12).

PRESSURE DISTRIBUTION IN VAPOR GAP

Evaluation of equation (B15) at the boundary defined by equation (11) gives

$$p(1, \theta^*) = p_a = -\cos\ \theta^*(20C_4 + 2C_2) + {}^3C \tag{D1}$$

where the dimensionless atmospheric pressure p_a is given as

$$p_a \equiv \frac{P_o}{\frac{\rho u^{*2}}{g_c}} \tag{D2}$$

Solving for the constant ${}^3C$ gives

$${}^3C = p_a + \cos\ \theta^*(20C_4 + 2C_2) \tag{D3}$$

Substituting equation (D3) back into equation (B15) gives for the pressure distribution

$$p(\zeta, \theta) = 20C_4(-\zeta\cos\ \theta + \cos\ \theta^*) + 2C_2\left(\frac{-\cos\ \theta}{\zeta^2} + \cos\ \theta^*\right) + p_a \tag{D4}$$

The pressure and velocity distributions which relate to the shearing stresses are

now substituted into the static force balance (eq. (12)) to determine the remaining constant. The static force balance is divided into four integrals so that the contribution of each term can be more easily visualized. Figure 2 shows a schematic of the pressure and shear forces acting on the sphere.

FORCES ACTING ON SPHERE

Pressure Force

The component of pressure force within the gap given by equation (12) is rewritten as

$$i_1 = \int_0^{2\pi} \int_0^{\theta^*} P(r, \theta)\big|_{r=R_o} \cos\theta \, R_o^2 \sin\theta \, d\theta \, d\Phi \tag{D5}$$

To nondimensionalize the weight as well as the components of force, the parameter w^* is defined as

$$w^* \equiv \frac{\rho u^{*2} R_o^2}{g_c} \tag{B25}$$

Dividing equation (D5) by equation (B25) gives

$$I_1 = \frac{i_1}{w^*} = \int_0^{2\pi} \int_0^{\theta^*} \frac{P(r, \theta)\big|_{r=R_o} \cos\theta \, R_o^2 \sin\theta \, d\theta \, d\Phi}{w^*} \tag{D6}$$

However, since

$$\frac{P(r, \theta)}{w^*} = \frac{p(\zeta, \theta)}{R_o^2} \tag{D7}$$

equation (D6) becomes

$$I_1 = \int_0^{2\pi} \int_0^{\theta^*} p(\zeta, \theta)\big|_{\zeta=1} \cos\theta \sin\theta \, d\theta \, d\Phi \tag{D8}$$

Evaluating this integral gives

$$I_1 = 4\pi\left[(10C_4 + C_2)\left(-\frac{1}{3} + \frac{1}{2}\cos\theta^* - \frac{1}{6}\cos^3\theta^*\right) + \frac{p_a}{4}(1 - \cos^2\theta^*)\right] \tag{D9}$$

Tangential Shear Force

The component of force due to tangential shear in the static force balance is given as

$$i_2 = -\int_0^{2\pi}\int_0^{\theta^*} \tau_{r\theta}\sin\theta\Big|_{r=R_o} R_o^2 \sin\theta\, d\theta\, d\Phi \tag{D10}$$

Nondimensionalizing this equation gives

$$I_2 = \frac{i_2}{w^*} = -\int_0^{2\pi}\int_0^{\theta^*} \frac{\tau_{r\theta}}{w^*}\sin\theta\Big|_{r=R_o} R_o^2 \sin\theta\, d\theta\, d\Phi \tag{D11}$$

But

$$\tau_{\zeta\theta} = \frac{\tau_{r\theta}}{w^*} = -\frac{\mu u^*}{g_c R_o w^*}\left[\zeta\frac{\partial}{\partial\zeta}\left(\frac{v_\theta}{\zeta}\right) + \frac{1}{\zeta}\frac{\partial v_\zeta}{\partial\theta}\right] \tag{D12}$$

However,

$$\frac{\mu u^*}{g_c R_o w^*} = \frac{\mu}{\rho u^* R_o R_o^2} = \frac{1}{Re R_o^2} = \frac{1}{R_o^2} \tag{D13}$$

since the Reynolds number is identically 1. Thus,

$$I_2 = \int_0^{2\pi}\int_0^{\theta^*} \left[\zeta\frac{\partial}{\partial\zeta}\left(\frac{v_\theta}{\zeta}\right) + \frac{1}{\zeta}\frac{\partial v_\zeta}{\partial\theta}\right]\Bigg|_{\zeta=1} \sin^2\theta\, d\theta\, d\Phi \tag{D14}$$

Substituting the values of $v_\theta(1, \theta)$ and $v_\zeta(1, \theta)$ into equation (D14) and integrating yield

$$I_2 = -12\pi(C_1 + C_4)\left[\frac{\cos\theta^*}{3}(\sin^2\theta^* + 2) - \frac{2}{3}\right] \tag{D15}$$

Normal Shear Force

The normal component of shearing force acting on the sphere is given by

$$i_3 = \int_0^{2\pi}\int_0^{\theta^*} \tau_{rr}\cos\theta\big|_{r=R_o} R_o^2 \sin\theta\, d\theta\, d\Phi \tag{D16}$$

Nondimensionalizing this equation gives

$$I_3 = \frac{i_3}{w^*} = \int_0^{2\pi}\int_0^{\theta^*} \frac{\tau_{rr}}{w^*}\cos\theta\big|_{r=R_o} R_o^2 \sin\theta\, d\theta\, d\Phi \tag{D17}$$

But

$$\tau_{\zeta\zeta} = \frac{\tau_{rr}}{w^*} = \frac{-2\mu u^*}{w^* g_c R_o}\frac{\partial v_\zeta}{\partial\zeta} = \frac{-2}{R_o^2}\frac{\partial v_\zeta}{\partial\zeta} \tag{D18}$$

Therefore, equation (D17) can now be rewritten as

$$I_3 = -\int_0^{2\pi}\int_0^{\theta^*} \frac{\partial v_\zeta}{\partial\zeta}\bigg|_{\zeta=1} \cos\theta\sin\theta\, d\theta\, d\Phi \tag{D19}$$

and since $\partial v_\zeta/\partial\zeta\big|_{\zeta=1} = 0$,

$$I_3 = 0 \tag{D20}$$

Ambient Pressure Force

The ambient pressure acting on the upper portion of the sphere becomes

$$i_4 = \int_0^{2\pi} \int_{\pi}^{\theta^*} P_o \cos\theta R_o^2 \sin\theta \, d\theta \, d\Phi \tag{D21}$$

Nondimensionalizing and integrating gives

$$I_4 = \pi p_a (1 - \cos^2\theta^*) \tag{D22}$$

SUMMATION OF FORCES

Summing these dimensionless forces acting on the sphere gives

$$\frac{W_d}{w^*} = I_1 + I_2 - I_3 - I_4 \tag{D23}$$

or, after substituting in the values of I_1 to I_4

$$-\frac{W_d}{4\pi w^* C_4} = \left[\frac{1}{3}\left(10 + \frac{C_2}{C_4}\right) - 2\left(1 + \frac{C_1}{C_4}\right)\right]\left(1 - \frac{3}{2}\cos\theta^* + \frac{1}{2}\cos^3\theta^*\right) \tag{D24}$$

Now C_1 and C_2 are known values of C_4; however, θ^* is still an unknown.

$$C_4 = -\left(\frac{W_d}{8\pi w^*}\right)\frac{1 + \varphi + 4\varphi^2}{\left[1 + \varphi + \varphi^2 + 6(\varphi^3 + \varphi^4)\right] g(\theta^*)} \tag{D25}$$

where

$$g(\theta^*) \equiv 1 - \frac{3}{2}\cos\theta^* + \frac{1}{2}\cos^3\theta^* \tag{D26}$$

Based on experimental observations of water drops floating on liquid nitrogen, it seems that θ^* is near $\pi/2$. Thus, for θ^* near $\pi/2$, equation (D25) simplifies to

$$C_4 = -\left(\frac{W_d}{8\pi w^*}\right)\frac{1 + \varphi + 4\varphi^2}{1 + \varphi + \varphi^2 + 6(\varphi^3 + \varphi^4)} \tag{D27}$$

APPENDIX E

STATIC PRESSURE BALANCE FOR TRANSFORMATION T_2 (WHERE $\theta^* < \pi$)

PRESSURE DISTRIBUTION IN VAPOR GAP

The pressure distribution within the gap is obtained from the solution of the momentum equations (appendix D). It is given by equation (C14) as

$$\frac{p(\zeta, \theta)}{C_4} = \frac{-3(1 + \varphi)}{\zeta} - 6 \ln \zeta + 12 \ln\left(\sec \frac{\theta}{2}\right) + \frac{{}^3C}{C_4} \tag{C14}$$

where ${}^3C$ and C_4 are constants. The purpose of this appendix is to determine these constants subject to the boundary conditions

$$\text{Weight of sphere} = \int_A P\vec{n} \cdot d\vec{A} \tag{E1}$$

and

$$\left.\begin{aligned} (\zeta, \theta) &\rightarrow (1, \theta^*) \\ p &\rightarrow p_a \end{aligned}\right\} \tag{E2}$$

Applying condition (E2) to equation (C14) gives

$$\frac{p_a}{C_4} = -3(1 + \varphi) + 12 \ln\left(\sec \frac{\theta^*}{2}\right) + \frac{{}^3C}{C_4} \tag{E3}$$

or

$$\frac{{}^3C}{C_4} = \frac{p_a}{C_4} + 3(1 + \varphi) - 12 \ln\left(\sec \frac{\theta^*}{2}\right) \tag{E4}$$

Substituting equation (E4) into equation (C14) gives

$$\frac{p(\zeta, \theta) - p_a}{C_4} = -3(1 + \varphi)\left(\frac{1}{\zeta} - 1\right) - 6 \ln \zeta + 12 \ln\left(\frac{\sec \frac{\theta}{2}}{\sec \frac{\theta^*}{2}}\right) \tag{E5}$$

The remaining constant C_4 may now be determined from the static force balance (eq. (E1) or eq. (12)).

FORCES ACTING ON SPHERE

Pressure Force

The force component due to pressure is given by

$$i_1 = \int_0^{2\pi} \int_0^{\theta^*} P(r, \theta)\big|_{r=R_o} \cos\theta \, R_o^2 \sin\theta \, d\theta \, d\Phi \tag{E6}$$

In nondimensional form, equation (E6) becomes

$$I_1 = \frac{i_1}{w^*} = \int_0^{2\pi} \int_0^{\theta^*} p(\zeta, \theta)\big|_{\zeta=1} \cos\theta \sin\theta \, d\theta \, d\Phi \tag{E7}$$

where w^* is given by equation (B25). Evaluating this integral using equation (E5) gives

$$I_1 = +2\pi C_4 \int_0^{\theta^*} \left[12 \ln\left(\frac{\sec\frac{\theta}{2}}{\sec\frac{\theta^*}{2}} \right) + \frac{p_a}{C_4} \right] \cos\theta \sin\theta \, d\theta \tag{E8}$$

or

$$I_1 = 2\pi C_4 \left[-\frac{p_a}{2C_4} (\cos^2\theta^* - 1) - \frac{3}{2} \cos^2\theta^* + 3 \cos\theta^* - \frac{3}{2} \right] \tag{E9}$$

Tangential Shear Force

The tangential shear component is given by

$$i_2 = -\int_0^{2\pi} \int_0^{\theta^*} \tau_{r\theta} \sin\theta\big|_{r=R_o} R_o^2 \sin\theta \, d\theta \, d\Phi \tag{E10}$$

In nondimensional form, equation (E10) becomes

$$I_2 = \frac{i_2}{w^*} = -\int_0^{2\pi}\int_0^{\theta^*} \tau_{\zeta,\theta} \sin\theta\big|_{\zeta=1} \sin\theta \, d\theta \, d\Phi \tag{E11}$$

and substituting for $\tau_{\zeta,\theta}$, equation (E11) becomes

$$I_2 = \int_0^{2\pi}\int_0^{\theta^*} \left[\zeta \frac{\partial}{\partial\zeta}\left(\frac{v_\theta}{\zeta}\right) + \frac{1}{\zeta}\frac{\partial v_\zeta}{\partial\theta}\right]_{\zeta=1} \sin^2\theta \, d\theta \, d\Phi \tag{E12}$$

Evaluating the integrand and recalling that

$$v_\theta = \frac{F_2' \tan\frac{\theta}{2}}{\zeta} \tag{E13}$$

where $F_2'(1, \theta) = 0$, and

$$F''(1, \theta) = 2C_3 + 6C_4\zeta\big|_{\zeta=1} = [-3(1 + \varphi) + 6]C_4 \tag{E14}$$

then

$$I_2 = 6\pi C_4(1 - \varphi)\left(\frac{\cos^2\theta^*}{2} - \cos\theta^* + \frac{1}{2}\right) \tag{E15}$$

Normal Shear Force

The normal shear force acting on the sphere is given by

$$i_3 = \int_0^{2\pi}\int_0^{\theta^*} \tau_{rr} \cos\theta\big|_{r=R_o} R_o^2 \sin\theta \, d\theta \, d\Phi \tag{E16}$$

Now nondimensionalize equation (E16) using equation (B25) and recall that from equation (D18)

$$\tau_{\zeta\zeta} = \frac{\tau_{rr}}{w^*} = -\frac{2}{R_o^2}\frac{\partial v_\zeta}{\partial \zeta} \tag{E17}$$

Evaluating this derivative at $\zeta = 1$,

$$\left.\frac{\partial v_\zeta}{\partial \zeta}\right|_{\zeta=1} = 2\left.\frac{F}{\zeta^3} - \frac{F'}{\zeta^2}\right|_{\zeta=1} = 0 \tag{E18}$$

leads to the trivial result

$$I_3 = 0 \tag{E19}$$

Ambient Pressure Force

The ambient pressure acting on the upper portion of the sphere becomes

$$i_4 = \int_0^{2\pi}\int_{\pi}^{\theta^*} p_a \cos\theta R_o^2 \sin\theta \, d\theta \, d\Phi \tag{E20}$$

Nondimensionalizing and integrating

$$I_4 = \pi p_a(1 - \cos^2\theta^*) \tag{E21}$$

SUMMATION OF FORCES

Summing the forces acting on the sphere gives

$$\frac{W_d}{w^*} = I_1 + I_2 - I_3 - I_4 \tag{E22}$$

Substituting in the values of equations (E9), (E15), (E19), and (E21), and assuming Δ to be small gives

$$-\frac{W_d}{3\pi w^* C_4} = (\cos^2\theta^* - 2\cos\theta^* + 1)\varphi \tag{E23}$$

Now, solving for C_4,

$$C_4 = -\frac{\dfrac{W_d}{3\pi w^*}}{\cos^2\theta^* - 2\cos\theta^* + 1} \tag{E24}$$

Equation (E5) may now be written as

$$p(\zeta, \theta) - p_a = -\left[-3(1+\varphi)\left(\frac{1}{\zeta} - 1\right) - 6\ln\zeta + 12\ln\left|\frac{\cos\frac{\theta^*}{2}}{\cos\frac{\theta}{2}}\right|\right]\frac{\dfrac{W_d}{3\pi w^*}}{f(\theta^*)} \tag{E25}$$

where

$$f(\theta^*) = \cos^2\theta^* - 2\cos\theta^* + 1 \tag{C30}$$

Now that C_4 is known, the velocity profiles are also known.

APPENDIX F

SOLUTION OF ENERGY EQUATION (NO CONVECTION)

Nondimensionalizing the Laplace form of the energy equation with no Φ dependence due to symmetry gives

$$\nabla^2\Theta = \frac{1}{\zeta^2}\frac{\partial}{\partial\zeta}\left(\zeta^2\frac{\partial\Theta}{\partial\zeta}\right) + \frac{1}{\zeta^2\sin\theta}\frac{\partial}{\partial\theta}\left(\sin\theta\frac{\partial\Theta}{\partial\theta}\right) = 0 \tag{F1}$$

where

$$\Theta = \frac{T - T_d}{T_s - T_d} \tag{F2}$$

SOLUTION OF $\nabla^2\Theta$

The boundary conditions are defined such that the temperature at the evaporating interface is at the saturation temperature

$$T = T_s \qquad \text{(evaporating interface)} \tag{9}$$

and the temperature of the opposite surface follows a cosine distribution,

$$T = T_d - \Delta T\cos\theta \qquad \text{(nonevaporating surface)} \tag{8}$$

In nondimensional form, the boundary conditions given by equations (8) and (9) for an evaporating supporting liquid become

$$\Theta(\varphi,\theta) = 1 \tag{F3}$$

$$\Theta(1,\theta) = -\epsilon\cos\theta \tag{F4}$$

where ϵ represents some fraction of the overall temperature difference (i.e., $\Delta T = \epsilon(T_d - T_s)$).

Solving equation (F1) subject to equations (F3) and (F4) gives the temperature distribution in the vapor gap

$$\Theta = \frac{\varphi}{\Delta}\left(1 - \frac{1}{\zeta}\right) + \frac{\epsilon}{\varphi^3 - 1}\left(\zeta - \frac{\varphi^3}{\zeta^3}\right)\cos\theta \qquad \text{(general solution)} \tag{F5}$$

For sufficiently small ϵ, equation (F5) reduces to the radial conduction solution with the constant-temperature boundary condition

$$\Theta(1,\theta) = 0 \tag{F6}$$

$$\Theta(\varphi,\theta) = 1 \tag{F3}$$

$$\Theta = \frac{\varphi}{\Delta}\left(1 - \frac{1}{\zeta}\right) \qquad \text{(radial conduction dominant)} \tag{F7}$$

SOLUTION OF $\nabla^2\Theta_c$, $\theta^* < \pi/2$

The solutions (eqs. (F5) and (F7)) are not dependent at this point on the position of the interface angle θ^*. However, one important case to consider is a solution of equation (F1) for $\theta^* < \pi/2$ subject to a different but similar set of boundary conditions

$$\Theta_c(1,\theta) = \epsilon\frac{\cos\theta}{\cos\theta_{ref}} \tag{F8}$$

$$\Theta_c(\varphi,\theta) = 0 \tag{F9}$$

where ϵ is an arbitrary positive constant, $\epsilon > 0$, which is at the disposal of the experimentalist and/or theoretician, and

$$\Theta_c = \frac{T - T_s}{(T_d)_{ref} - T_s} \tag{F10}$$

$$0 \le \theta_{ref} \le \theta^* < \frac{\pi}{2} \tag{F11}$$

(Note: $\Theta_c \neq \Theta$.) Solving equation (F1) subject to the boundary conditions (F8) to (F11) gives the temperature distribution in the vapor gap

$$\Theta_c = -\frac{\epsilon}{\varphi^3 - 1}\left(\zeta - \frac{\varphi^3}{\zeta^2}\right)\frac{\cos\theta}{\cos\theta_{ref}} \qquad \text{for } \theta^* < \frac{\pi}{2} \tag{F12}$$

Equation (F8) represents a θ-dependent variation in surface temperature confined to those cases where the floating interface angle $\theta^* < \pi/2$. Furthermore, a form similar to equation (F12) can be obtained from equation (F5) by assuming ϵ sufficiently large, which reflects the strong θ-dependent surface-temperature condition.

The advantage of equation (F12) is, as pointed out in appendix B, that for the special case of $\theta^* < \pi/2$ a similarity solution is attained. One disadvantage of permitting a θ-dependent surface-temperature variation (eqs. (F4) and (F8)) is that neither ϵ nor θ_{ref} is known a priori and must be assumed or dictated by the experiment. The major advantage of the constant-temperature solution (eq. (F7)) is its simplicity, but it requires the assumption of the average or representative surface temperature.

APPENDIX G

EFFECT OF CONVECTION ON ENERGY EQUATION

While the convection effects are analyzed for the case where $\psi_1 = F_1 \sin^2 \theta$ and $\theta^* < \pi/2$, the results are not expected to significantly deviate for the case where $\psi_2 = F_2(1 - \cos \theta)$.

If the flow in the θ-coordinate is assumed to approximate the fully developed case (i.e., $\partial T/\partial \theta$ is negligible and radial conduction dominates) and viscous dissipation to be small, the energy equation reduces to

$$v_\zeta \frac{\partial \Theta}{\partial \zeta} = \frac{1}{Pr} \frac{1}{\zeta^2} \frac{\partial}{\partial \zeta} \left(\zeta^2 \frac{\partial \Theta}{\partial \zeta} \right) \tag{G1}$$

where

$$\Theta = \frac{T - T_d}{T_s - T_d} \tag{G2}$$

If the convection terms on the right side of equation (G1) were neglected, the energy equation would reduce to the pure conduction equation given by equation (F7) in appendix F of this report.

Equation (G1) may be rearranged to give

$$\frac{v_\zeta Pr}{\zeta^2} = \frac{1}{\zeta^2} \frac{\partial}{\partial \zeta} \left[\ln \left(\zeta^2 \frac{\partial \Theta}{\partial \zeta} \right) \right] \tag{G3}$$

Integrating equation (G3) over Φ, θ, ζ gives

$$\int \int_{\Phi=0}^{2\pi} \int_{\theta=0}^{\theta^*} \left(\frac{v_\zeta Pr}{\zeta^2} \right) \zeta^2 \sin \theta \, d\theta \, d\Phi \, d\zeta$$

$$= \int \int_{\Phi=0}^{2\pi} \int_{\theta=0}^{\theta^*} \frac{1}{\zeta^2} \frac{\partial}{\partial \zeta} \left[\ln \left(\zeta^2 \frac{\partial \Theta}{\partial \zeta} \right) \right] \zeta^2 \sin \theta \, d\theta \, d\Phi \, d\zeta \tag{G4}$$

Substituting for v_ζ using equation (B3) and performing the integration indicated by equation (G4) gives

$$-\mathrm{Pr}(\cos\theta^* + 1)\int \frac{F(\zeta)}{\zeta^2}\,d\zeta = \ln\left({}^1C\,\zeta^2\,\frac{\partial\Theta}{\partial\zeta}\right) \tag{G5}$$

which represents the variation in Θ due to ζ where Θ has been averaged over θ and Φ. Solving for $\partial\Theta/\partial\zeta$ gives

$$\frac{\partial\Theta}{\partial\zeta} = \frac{1}{{}^1C\,\zeta^2}\exp\left[-\mathrm{Pr}(\cos\theta^* + 1)\int \frac{F(\zeta)}{\zeta^2}\,d\zeta\right] \tag{G6}$$

Integrating equation (G6) gives

$$\Theta = \frac{1}{{}^1C}\int_1^\zeta \frac{\exp\left[-\mathrm{Pr}(\cos\theta^* + 1)\int_1^\tau \frac{F(y)}{y^2}\,dy\right]}{\tau^2}\,d\tau + {}^2C \tag{G7}$$

The boundary conditions of temperature (eqs. (8) and (9)) can be rewritten in dimensionless form, where $\epsilon \to 0$ and $T \to T_d$, as

$$\Theta(1,\theta) = 0 \tag{F6}$$

$$\Theta(\varphi,\theta) = 1 \tag{F3}$$

Applying these boundary conditions to equation (G7) gives

$${}^2C = 0 \tag{G8}$$

$${}^1C = \int_1^\varphi \frac{\exp\left[-\mathrm{Pr}(\cos\theta^* + 1)\int_1^\tau \frac{F(y)}{y^2}\,dy\right]}{\tau^2}\,d\tau \tag{G9}$$

Therefore, the temperature distribution becomes

$$\Theta = \frac{\displaystyle\int_1^{\zeta} \frac{\exp\left[-\mathrm{Pr}(\cos\theta^* + 1)\displaystyle\int_1^{\tau}\frac{F(y)}{y^2}\,dy\right]}{\tau^2}\,d\tau}{\displaystyle\int_1^{\varphi} \frac{\exp\left[-\mathrm{Pr}(\cos\theta^* + 1)\displaystyle\int_1^{\tau}\frac{F(y)}{y^2}\,dy\right]}{\tau^2}\,d\tau} \tag{G10}$$

However, expanding the exponent in equation (G10) in a power series about 1 and performing the integration give

$$\Theta(\zeta) = \underbrace{\left(1 + \frac{1}{\Delta}\right)\left(1 - \frac{1}{\zeta}\right)}_{\text{Conduction}} \underbrace{\Lambda(\zeta, \Delta)}_{\substack{\text{Convection} \\ \text{correction}}} \tag{G11}$$

where

$$\Lambda(\zeta,\Delta) = \frac{1 + \dfrac{\zeta}{\zeta - 1}\displaystyle\int_1^{\zeta} \frac{1}{\tau^2}\sum_{K=1}^{N}\left[-\mathrm{Pr}(\cos\theta^* + 1)\int_1^{\tau}\frac{F(y)}{y^2}\,dy\right]^K d\tau}{1 + \dfrac{1+\Delta}{\Delta}\displaystyle\int_1^{\varphi} \frac{1}{\tau^2}\sum_{K=1}^{N}\left[-\mathrm{Pr}(\cos\theta^* + 1)\int_1^{\tau}\frac{F(y)}{y^2}\,dy\right]^K d\tau} \tag{G12}$$

The first term in equation (G11) is identical to the solution for pure conduction, while the $\Lambda(\zeta, \Delta)$ term accounts for convection effects. Conduction is assumed to dominate; thus $\Lambda(\zeta, \Delta)$ is taken to be 1. However, the range of applicability of this assumption is now considered.

Dividing equation (G10) by equation (G11) gives

$$\Lambda = \frac{\displaystyle\int_1^{\zeta} \frac{\exp\left[-\mathrm{Pr}(\cos\theta^* + 1)\displaystyle\int_1^{\tau}\frac{F(y)}{y^2}\,dy\right]}{\tau^2}\,d\tau}{\left(1+\frac{1}{\Delta}\right)\left(1-\frac{1}{\zeta}\right)\displaystyle\int_1^{\varphi}\frac{\exp\left[-\mathrm{Pr}(\cos\theta^* + 1)\displaystyle\int_1^{\tau}\frac{F(y)}{y^2}\,dy\right]}{\tau^2}\,d\tau} \tag{G13}$$

The parameter Λ was evaluated numerically (using double-precision arithmetic) by employing Simpson's rule to evaluate the integral in equation (G13). As a specific example, a plot of the numerical results is shown in figure 6 for $W_d/8\pi w^*$ equal to 0.472×10^6 (water drop on liquid nitrogen). The temperature distribution is shown to be greater than predicted from the conduction solution. This is expected, since the specific heat of the vapor prevents it from dropping to the value predicted by conduction alone. As shown in this figure, the conduction solution is within 10 percent of the actual temperature profile.

The slopes at the sphere surface ($\zeta - 1 = 0$), and at the supporting liquid surface ($\zeta - 1 = 0.04$), are a measure of the heat-transfer coefficient since the heat-transfer rate is, of course, proportional to the temperature gradient. As shown in figure 6, the gradient at the sphere surface is greater than that at the supporting liquid surface; that is, the heat-transfer coefficient from the sphere is greater than that to the supporting surface. This is expected: since all the heat leaving the sphere does not reach the supporting surface, some of it is convected away in the vapor stream.

The analytical expression for the temperature gradient at the drop surface can be found by differentiating equation (G11) and evaluating the derivative at $\zeta = 1$. This gives,

$$\left.\frac{\partial\Theta}{\partial\zeta}\right|_{\zeta=1} = \underbrace{(1+\Delta^{-1})}_{\text{Conduction}}\underbrace{\left[\frac{1}{1+\left(\frac{1+\Delta}{\Delta}\right)\displaystyle\int_1^{\varphi}\frac{1}{\tau^2}(\mathrm{SUM})\,d\tau}\right]}_{\text{Convection correction term}} \tag{G14}$$

where

$$\mathrm{SUM} = \sum_{K=1}^{\infty}\left[-\mathrm{Pr}(\cos\theta^* + 1)\int_1^{\tau}\frac{F(y)}{y^2}\,dy\right]^K \tag{G15}$$

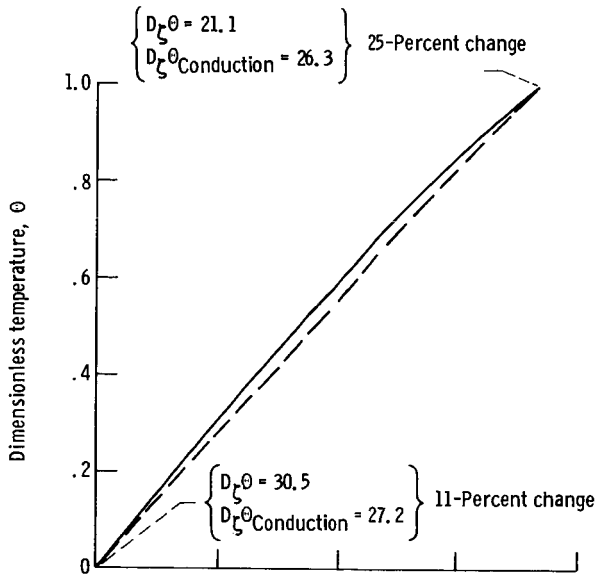

(a) Dimensionless temperature profile and gradients at boundaries. Dimensionless gap thickness, $\Delta = 0.0367$.

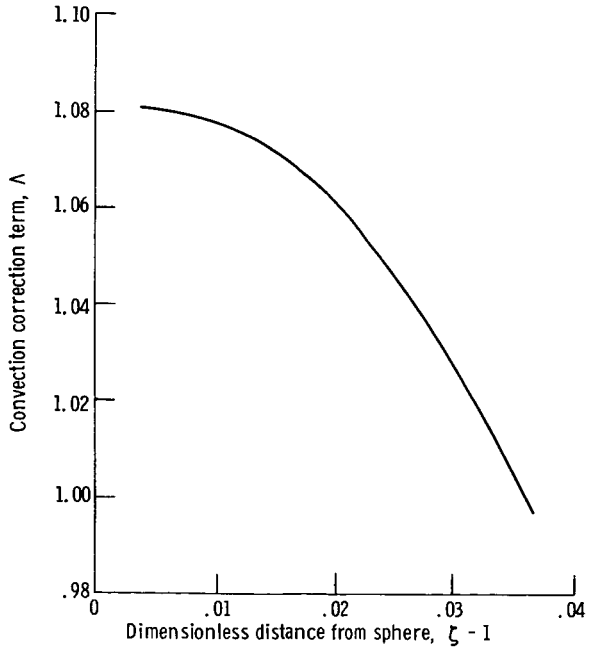

(b) Variation of convection correction term with distance from sphere.

Figure 6. - Numerical solution of energy equation. Data from sample calculation. (See appendix J.)

The magnitude of the convection term was evaluated numerically. This term required a 10-percent correction in the temperature gradient for the case where $Pr = 0.7$ and $\Delta = 0.04$. However, at the expense of accuracy and for increased simplification, the closed-form conduction solution was used in the analysis with λ replaced by λ^*,

$$\lambda^* = \lambda\left(1 + \frac{1}{2}\,\frac{C_p\,\Delta T}{\lambda}\right) \tag{G16}$$

which tends to correct for the convection omission.

APPENDIX H

SHAPE OF LIQUID-VAPOR INTERFACE

It has been shown that the sphere is supported by shear and pressure forces acting at the vapor-sphere interface, see appendixes D and E. In this appendix, it is demonstrated that the fluid possesses sufficient surface strength and buoyancy to restrain the shear and pressure forces acting at the vapor-liquid interface.

FORCES AT INTERFACE

Within the supporting liquid, there are two forces to be considered, buoyancy and surface tension. Buoyancy is composed of two terms: (1) fluid displacement by the sphere to an angle of θ^* and (2) fluid head as a result of fluid displacement by surface curvature. Each of these forces is now considered separately.

Surface-Tension Support

If a load is placed on an axisymmetric shell or membrane structure (see fig. 7), it

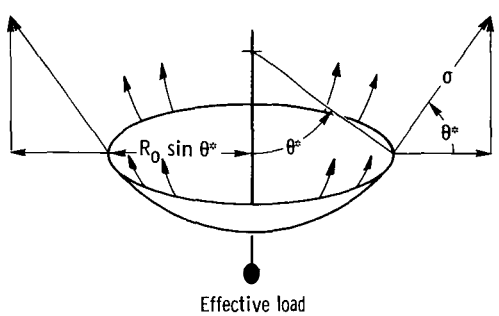

Figure 7. - Loading of axisymmetric shell or membrane.

is supported at the circular interface, or load circle. Here the effective load is supported by a component of surface tension

$$F_\sigma = 2\pi R_o \sigma \sin^2\theta^* \tag{H1}$$

F_σ may also be found by simply integrating the lift component of the surface-tension pressure rise over the shell, that is,

$$F_\sigma = \int_0^{2\pi} \int_0^{\theta^*} \left(\frac{2\sigma}{R_o}\right) R_o^2 \cos\theta \sin\theta \, d\theta \, d\Phi \tag{H1a}$$

Fluid Displacement by Sphere

The "pressure forces" acting on the spherical interface are illustrated in figure 8.

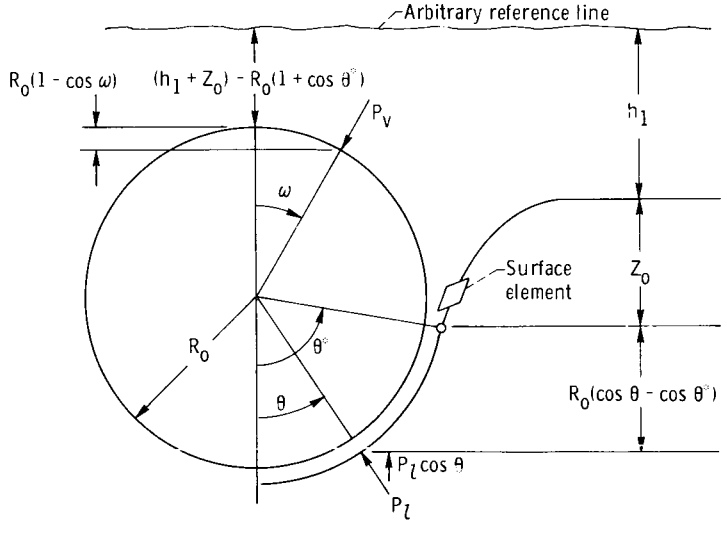

Figure 8. - Forces acting at vapor-liquid interface. Fluid displacement by sphere.

The buoyancy resulting from these forces is obtained by integration; however, it must be noted that θ^* and Z_o, while constants, are also unknown and must be determined from the force balance and interface curvature

$$F_b = \int_0^{2\pi} \int_0^{\theta^*} P_l \cos\theta \, dA_1 - \int_0^{2\pi} \int_0^{\pi-\theta^*} P_v \cos\theta \, dA_2 \tag{H2}$$

$$F_b = 2\pi \int_0^{\theta^*} \left\{ h_1 \rho \frac{g}{g_c} + \left[Z_o + R_o(\cos\theta - \cos\theta^*) \right] \rho_l \frac{g}{g_c} \right\} \cos\theta \, R_o^2 \sin\theta \, d\theta$$

$$- 2\pi \int_0^{\pi - \theta^*} \left\{ \rho \frac{g}{g_c} \left[h_1 + Z_o - R_o(1 + \cos\theta^*) \right] + \rho \frac{g}{g_c} R_o(1 - \cos\omega) \right\} R_o^2 \sin\omega \, d\omega \quad \text{(H3)}$$

Integrating equation (H3) gives the buoyancy in terms of θ^* and Z_o as

$$F_b = \pi(\rho_l - \rho) \frac{g}{g_c} R_o^2 \left\{ 2R_o \left[\frac{\rho_l + \rho}{3(\rho_l - \rho)} - \frac{\cos\theta^*}{2} + \frac{\cos^3\theta^*}{6} \right] + Z_o(1 - \cos^2\theta^*) \right\} \quad \text{(H4)}$$

If $(\rho_l - \rho) \rightarrow \rho_l$, which is true for most film boiling cases, $\left[(\rho_l + \rho)/(\rho_l - \rho) \right] \rightarrow 1$.

Fluid Displacement by Interface Curvature

As θ increases beyond θ^*, the vapor gap between the sphere and the liquid becomes very large. This implies that the pressure acting on the interface approaches atmos-

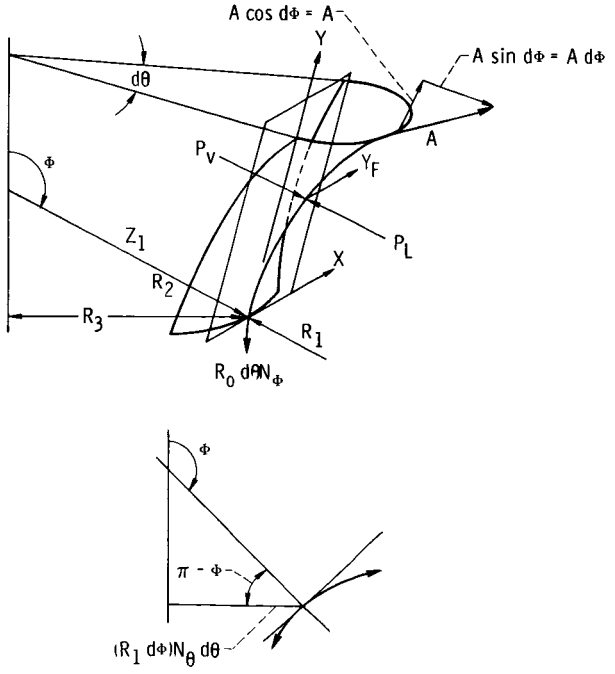

Figure 9. - Forces acting on a thin shell or membrane.

pheric; however, the pressure on the liquid side of the interface is above atmospheric and must be balanced by curvature of the interface.

Consider an element of the axisymmetric surface of figure 8 as shown in figure 9. Let the surface forces per unit length in the Φ- and θ-directions be designated as N_Φ and N_θ, respectively. Let there be an X-Y plane tangent to the surface at some point P. Let Z be the coordinate colinear with the radii of curvature R_1 and R_2.

The force A is a result of a change in R_3 and N_Φ with respect to Φ:

$$A = \left(R_3 + \frac{\partial R_3}{\partial \Phi} d\Phi\right) d\theta \left(N_\Phi + \frac{\partial N_\Phi}{\partial \Phi} d\Phi\right) \tag{H5}$$

Resolving the forces as shown in figure 9 and neglecting second-order terms results in the force balances for Y- and Z-forces.

Y-forces. - The Y-force balance equation is

$$\frac{\partial R_3 N_\Phi}{\partial \Phi} d\Phi\, d\theta - (R_1 N_\theta\, d\theta\, d\Phi) \cos(\pi - \Phi) + Y_F\, d\Phi\, d\theta = 0 \tag{H6}$$

where Y_F is some surface force acting in the Y-direction.

Z-forces. - The Z-force balance equation is

$$-R_3 N_\Phi\, d\theta\, d\Phi + (R_1 N_\theta\, d\Phi\, d\theta) \sin(\pi - \Phi) + (P_l - P_v) R_3 R_1\, d\Phi\, d\theta = 0 \tag{H7}$$

where $(P_l - P_v)\, dA$ is the arbitrary force acting in the Z-direction.

If $Y_F \equiv 0$ and $P - P_v \equiv \Delta P$, equations (H6) and (H7) become

$$\frac{\partial R_3 N_\Phi}{\partial \Phi} = -R_1 N_\theta \cos \Phi \tag{H8}$$

$$\frac{N_\Phi}{R_1} - \frac{N_\theta}{R_3} \sin \Phi = \Delta P \tag{H9}$$

Now $R_3 = R_2 \sin(\pi - \Phi)$, and substitution into equation (H9) would lead to a description of the surface in terms of the radii of curvature, R_1 and R_2.

For this report, we consider a surface of constant strength, $N_\Phi = N_\theta = \sigma = \text{Constant}$, being depressed by a nonwetting object; that is, a sphere of water depressing liquid nitrogen in the film-boiling regime. The problem is to solve these equations where Z_o

and θ^* are unknowns. This requires an iterative-matching solution where the first step is to solve equations (H8) and (H9) subject to a given Z_o and θ^*. The second step is to determine if such a θ^* and Z_o will yield sufficient strength to support the sphere. Although in nature the solution is unique, the computer results may not be unique in that a family of approximate solutions may exist near the unique solution. (This could also indicate that nature is not unique.) Recasting equations (H8) and (H9) by substituting

$$u = \sin \Phi \tag{H10}$$

and nondimensionalizing by the characteristic length

$$L^2 = \frac{(\rho_l - \rho)g}{\sigma g_c} \tag{H11}$$

which arises in a natural way from equation (H9), give

$$D_x u = -\frac{u}{x} - z \tag{H12}$$

$$D_x z = \tan \Phi = \frac{u}{\pm\sqrt{1 - u^2}} \tag{H13}$$

where

$$z = \frac{Z}{L} \tag{H14}$$

$$x = \frac{R_o}{L} \tag{H15}$$

For $\theta^* > \pi/2$, $\tan \Phi > 0$, and the sign in equation (H13) is positive; for $\theta^* < \pi/2$, $\tan \Phi < 0$, and the sign in equation (H13) is negative.

Anticipating the computer solution, the increments are written

$$u_{j+1} = u_j + (D_x u)\,\Delta x \tag{H16}$$

$$z_{j+1} = z_i + (D_x z)\,\Delta x \tag{H17}$$

Computer solution. - As the initial conditions are assumed to be known (i.e., Z_o, θ^*, and the slope of the interface), a fourth-order Runge-Kutta routine was applied to equations (H12) and (H13) subject to equations (H16) and (H17). (The Runge-Kutta routine was developed by Paul Swiegert and is obtainable on loan from Lewis.) The resulting axisymmetric profile, shown in figure 10, represents the fluid displaced by interface curvature. The problem now becomes one of determining the Z_o and θ^* which not only result in a balance of forces but yield $\sin \Phi = 0$ at $Z/L = 0$.

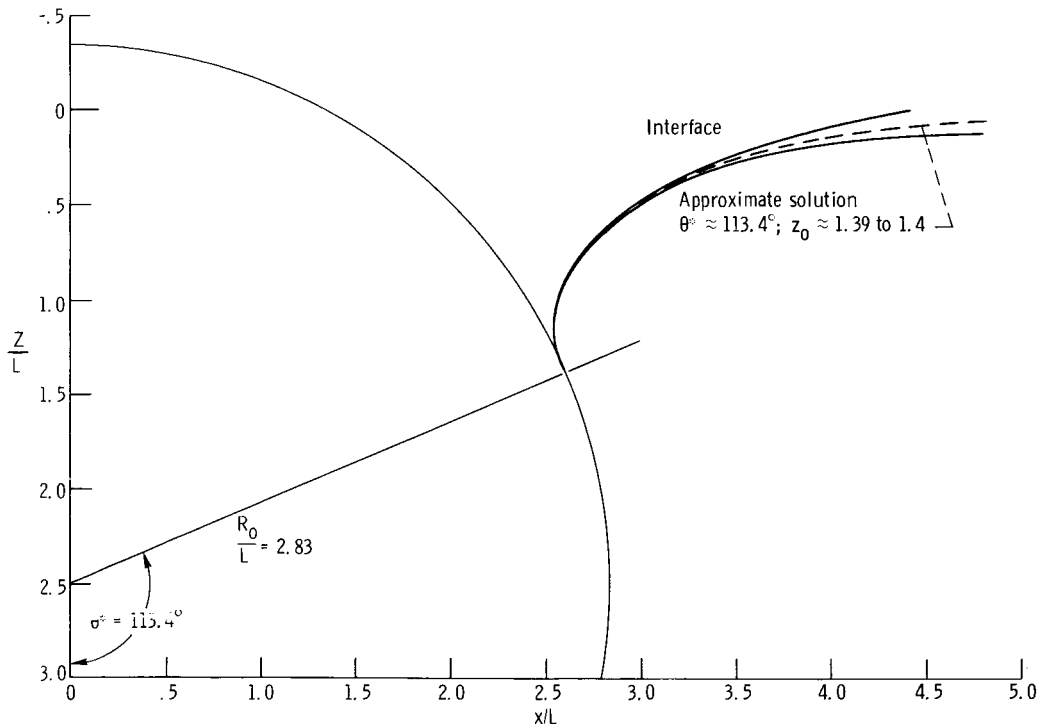

(a) Enlargement of section of (b).

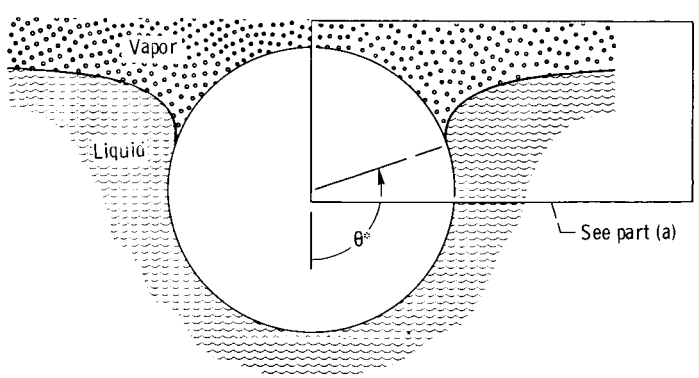

(b) Schematic model for interface configuration.

Figure 10. - Interface configuration for water sphere on liquid nitrogen. Radius of sphere, R_o = 0.3 centimeter; density, $\rho_l - \rho$ = 0.8 gram per cubic centimeter; sphere density, ρ_d = 1.0 gram per cubic centimeter; surface tension, σ = 8.8 dynes per centimeter.

BALANCE OF FORCES

The forces for a given z_o and θ^* must balance the weight of the sphere. This requires an iterative procedure supplying new z_o and θ^* values to achieve the desired balance

$$\frac{4}{3}\pi\rho_s \frac{g}{g_c} R_o^3 = F_b + F_\sigma \tag{H18}$$

Herein the solution was attained only for the case,

$$R_o = 0.3 \text{ cm}$$

$$\rho_l - \rho = 0.8 \text{ g/cc}$$

$$\rho_s = 1.0 \text{ g/cc}$$

$$\sigma = 8.8 \text{ dynes/cm}$$

which is shown as figure 10. While the forces are balanced to less than 0.3 percent, the exact solution was not obtained. The interface is bounded by the given curves: one where $z \to 0$ but $\sin \Phi > 0$, and one where $\sin \Phi \to 0$ but $z > 0$; and the interface was interpolated from these curves. In this case, θ^* is approximately $113\frac{1}{2}^\circ$, and the initial head is approximately 0.148 centimeter. This case was chosen because it is representative of the floating spheres of table I, and visual examination of these spheres, along with motion pictures, appears to confirm the prediction (see motion-picture supplement C-267).

At the time of publication of this report, a more elegant technique for determining an axisymmetric interface was found in the paper by Huh and Scriven (ref. 12).

APPENDIX I

FREEZING TIME: ANALYTICAL MODEL

An experimental check on the theoretical solution requires an estimation of the time required to freeze a sphere of liquid. However, there are many facets of the freezing problem that we do not understand. For example, the convective heat-transfer coefficient from the top of the sphere, as well as internal convection, is unknown. If subcooling occurs (and up to $T_d - T_f = -40$ K is possible), the solid will not form at the freezing temperature, which completely alters a heat balance. The compressive effects of freezing on the interface freezing temperature and interface growth rate are not known; the effects of cracks, ice "worms," and the 4° C inversion point are also unknown. To what extent does eccentric cooling and freezing alter a concentric-sphere freezing analysis? The effect of a pseudo-steady-state analysis, as compared to a complete transient analysis, is difficult to assess. To what extent is the metastable Leidenfrost phenomenon influencing the results? If a sphere followed the metastable Leidenfrost line (ref. 4), floating times would be greatly extended.

Each of these unknowns constitutes a report in itself. As a first-order cut at the problem, a pseudo-steady-state model is assumed; the model is illustrated in figure 11.

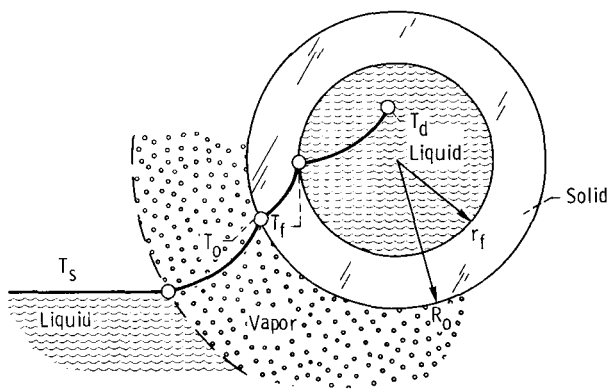

Figure 11. - Schematic model of freezing drop.

Obviously omitted are such effects as subcooling, convection, compression, 4° C inversion, eccentricity, the transient nature, and cracks. The equation depicting the energy distribution within the concentric solid region is

$$\left(\rho C_p \overline{V}_r\right)_{solid} \frac{\partial T}{\partial r} = \frac{k_{solid}}{r^2} \frac{\partial}{\partial r}\left(r^2 \frac{\partial T}{\partial r}\right) \tag{I1}$$

(While it must be readily admitted that freezing does not occur in a concentric manner, the inclusion of the noncencentric effects is difficult and seems unwarranted.) However, if it is assumed that $\overline{V}_r$ is small, energy is transported by conduction, and equation (I1) can be written

$$\frac{\partial}{\partial \zeta}\left(\zeta^2 \frac{\partial \Gamma}{\partial \zeta}\right) = 0 \tag{I2}$$

subject to the boundary conditions

$$\zeta = 1, \qquad \Gamma = \frac{T - T_o}{T_f - T_o} = 0$$

$$\zeta = 1 - \beta, \qquad \Gamma = 1 \tag{I3}$$

where

$$\beta = 1 - \frac{r_f}{R_o} \tag{I4}$$

The solution of equation (I2) subject to equation (I3) is

$$\Gamma = \left(\frac{\beta - 1}{\beta}\right)\left(1 - \frac{1}{\zeta}\right) \tag{I5}$$

The heat flow out of the sphere may be written as

$$q_r = h_d(T_o - T_s) = h_{ice}(T_f - T_o) \tag{I6}$$

Solving equation (I6) for T_o gives

$$T_o = \frac{T_s h_d + h_{ice} T_f}{h_{ice} + h_d} \tag{I7}$$

and using equation (I7) in determing Q_R yields

$$Q_R = q_r A = 4\pi R_o^2 h_d \frac{T_f - T_s}{1 + \frac{h_d}{h_{ice}}} \tag{I8}$$

From equation (I5)

$$\left.\frac{\partial \Gamma}{\partial \zeta}\right|_{\zeta=1} = \frac{\beta - 1}{\beta} = -\frac{1}{\frac{R_o}{r_f} - 1} \tag{I9}$$

Using equations (I9) and (I6) results in

$$h_{ice} = \frac{q_r}{T_f - T_o} = \frac{-k_{ice}}{R_o} \left.\frac{\partial \Gamma}{\partial \zeta}\right|_{\zeta=1} = \frac{k_{ice}}{R_o \left(\frac{R_o}{r_f} - 1\right)} \tag{I10}$$

Substituting equation (I10) into equation (I8) yields the following form for Q_R

$$Q_R = \frac{4\pi R_o^2 (T_f - T_s) h_d}{1 + \left(\frac{R_o}{r_f} - 1\right) \frac{R_o h_d}{k_{ice}}} \tag{I11}$$

The interface energy balance gives the advance of the solid surface per unit time, which will give the desired freezing time

$$-\rho_{ice} \gamma \frac{dr_f}{dt} = \frac{-k_{ice}(T_f - T_o)}{R_o} \left.\frac{\partial \Gamma}{\partial \zeta}\right|_{\zeta=(r_f/R_o)} - h_l (\overline{T}_d - T_f) \tag{I12}$$

Here $\overline{T}_d$ represents a suitable time-averaged value, that is,

$$\overline{T}_d = \frac{(T_d)_o + T_f}{2} \tag{I13}$$

When equations (I5), (I10), and (I11) are substituted into equation (I12), the interface velocity becomes

$$-\frac{dr_f}{dt} = \frac{h_d(T_f - T_s)}{\rho_{ice}\gamma}\left\{\frac{1}{\left(\frac{r_f}{R_o}\right)^2 + \frac{R_o h_d}{k_{ice}}\left[\frac{r_f}{R_o} - \left(\frac{r_f}{R_o}\right)^2\right]}\right\} - \frac{h_l}{\rho_{ice}\gamma}(\overline{T}_d - T_f) \tag{I14}$$

By defining the following constants:

$$^1C = 1 - \frac{R_o h_d}{k_{ice}} \tag{I15}$$

$$^2C = \frac{R_o h_d}{k_{ice}} \tag{I16}$$

$$^3C = \frac{-h_l}{\rho_{ice}\gamma R_o}(\overline{T}_d - T_f) \tag{I17}$$

$$^4C = \frac{h_d(T_f - T_s)}{\rho_{ice}\gamma R_o} \tag{I18}$$

equation (I14) may be written in a simplified form as

$$-\int_1^x \left(1 - \frac{^4C}{^1C\,^3Cx^2 + {}^2C\,^3Cx + {}^4C}\right) dx = \int_0^t {}^3C\, dy \tag{I19}$$

where $x = r_f/R_o$. Equation (I19) has two solutions, depending on the sign of the characteristic

$$C_R = \left({}^2C\,^3C\right)^2 - 4\,{}^1C\,^3C\,^4C \tag{I20}$$

Integrating equation (I19) gives the freezing time as

$$t = \begin{cases} -\frac{1}{{}^3C}\left(\frac{r_f}{R_o} - 1\right) + \frac{{}^4C}{{}^3C\sqrt{C_R}} \ln \left| \frac{2\,{}^1C{}^3C\left(\frac{r_f}{R_o}\right) + {}^2C{}^3C - \sqrt{C_R}}{2\,{}^1C{}^3C\left(\frac{r_f}{R_o}\right) + {}^2C{}^3C + \sqrt{C_R}} \times \frac{2\,{}^1C{}^3C + {}^2C{}^3C + \sqrt{C_R}}{2\,{}^1C{}^3C + {}^2C{}^3C - \sqrt{C_R}} \right| & C_R > 0 \\ -\frac{1}{{}^3C}\left(\frac{r_f}{R_o} - 1\right) + \frac{2\,{}^4C}{{}^3C\sqrt{-C_R}} \left(\arctan\left\{ \frac{{}^3C\left[2\,{}^1C\left(\frac{r_f}{R_o}\right) + {}^2C\right]}{\sqrt{-C_R}} \right\} - \arctan\left[\frac{{}^3C(2\,{}^1C + {}^2C)}{\sqrt{-C_R}} \right] \right) & \text{for } C_R < 0 \end{cases} \tag{I21}$$

If the effect of the liquid core is neglected (i.e., the time required to remove sensible heat is negligible relative to the latent heat removal time), the solution of equation (I14) for $\overline{T}_d = T_f$ becomes

$$t = \frac{\rho_{ice}\gamma R_o}{3h_d(T_d - T_s)} \left\{ 1 - \left(\frac{r_f}{R_o}\right)^3 + \frac{R_o h_d}{2k_{ice}} \left[1 - 3\left(\frac{r_f}{R_o}\right)^2 + 2\left(\frac{r_f}{R_o}\right)^3 \right] \right\} \tag{I22}$$

In comparing equations (I21) and (I22) it would seem well to check the necessity of including transport to the liquid core in the interface energy balance (eq. (I14)). It is also evident that, because of the pseudo-steady-state assumptions, the sensible heat of the liquid core could be extracted prior to the freezing time predicted by equation (I21). The actual time would be between that predicted by equations (I21) and (I22), depending on h_l and $\overline{T}_d - T_f$ in equation (I12).

As the surface temperature cools, the freezing interface advances toward $r = 0$, and the sphere begins to behave as a solid losing heat to the environment. The governing equation becomes

$$h_d A(T - T_s) = -(\rho C_p)_{ice} V_d \frac{\partial(T - T_s)}{\partial \tau} \tag{I23}$$

where

$$\tau = t - \tau_f \tag{I24}$$

And at $\tau = 0$, the surface temperature $T(0)$ as well as the elapsed time τ_f are, as yet, unknowns. The solution of equation (I23) becomes (for $h_d/(\rho C_p)_{ice} = \text{Constant}$)

$$\frac{T - T_s}{T(0) - T_s} = \exp\left[-\frac{h_d A}{(\rho C_p)_{ice} V_d}\tau\right] \tag{I25}$$

Solving for the time τ,

$$\tau = -\frac{R_o(\rho C_p)_{ice}}{3h_d} \ln\left[\frac{T - T_s}{T(0) - T_s}\right] \tag{I26}$$

In order to determine $T(0)$, the slopes of equations (I21) and (I23) are matched and the interface location r_f/R_o, the time τ_f, and the temperature $T(0)$ can be determined.

$$D_t(T - T_s)_{eq.\,(I21)} = D_t(T - T_s)_{eq.\,(I26)} \tag{I27}$$

The change in surface temperature with time is, using the chain rule and letting $T = T_o$,

$$D_t(T - T_s) = \left[D_{h_{ice}}(T_o - T_s)\right]\left[D_{(r_f/R_o)^{h_{ice}}}\right]\left[D_t\left(\frac{r_f}{R_o}\right)\right] \tag{I28}$$

where from equation (I10),

$$D_{(r_f/R_o)^{h_{ice}}} = \frac{k_{ice}}{R_o\left(\frac{r_f}{R_o}\right)^2\left(\frac{R_o}{r_f} - 1\right)^2} \tag{I29}$$

and by manipulating equation (I7) and substituting equation (I6),

$$D_{h_{ice}}(T_o - T_s) = \frac{T_f - T_o}{h_{ice} + h_d} \tag{I30}$$

and finally from equation (I14) comes $D_t(r_f/R_o)$. The slopes given by equations (I28) and (I23) are matched (eq. (I27)); and the location of the freezing interface r_f/R_o, the time τ_f, and the surface temperature $T(0)$ are now determined. An example appears in a appendix F.

Of particular interest is the time required for the surface temperature to reach the Leidenfrost temperature T_L. From equation (I26),

$$\tau_L = -\frac{R_o(\rho C_p)_{ice}}{3h_d} \ln\left[\frac{T_L - T_s}{T(0) - T_s}\right] \tag{I31}$$

Equation (I31), while limited by simplifying assumptions, gives an estimate of how long the sphere will float.

APPENDIX J

SAMPLE CALCULATIONS

In order to test the theoretical model, an experiment was performed using water and liquid nitrogen. The problem considered here is to calculate the observed changes in the characteristics of the sphere.

Consider a sphere, radius R_o, of dye-tinted water "floating" on a sea of liquid nitrogen. As the fluid within the sphere freezes, the color changes; it is estimated that at least a $0.1R_o$ layer of ice is required to make the color change vivid. Because the sphere of water must contact the nitrogen to generate its vapor cushion, the surface should become crystalline; that is, ice will form. The crystalline structure forms a nonuniform surface; ice spires protrude into the encapsulated liquid and into the vapor gap, thereby initiating an early destruction of the vapor cushion. This description serves only to remind the reader that these calculations are greatly simplified with respect to the physics of the problem. With these limitations in mind, consider an 0.305-centimeter sphere of water floating on liquid nitrogen, which possesses a θ^* of approximately $113\frac{1}{2}^{\circ}$, as is shown in appendix H and illustrated in figure 10 for $R_o = 0.3$ centimeter. Therefore, the heat-transfer coefficient will be calculated from equation (C25), $\theta^* < \pi$.

The water temperature at inception is 298 K, and the saturation temperature of liquid nitrogen is 77.4 K. The drop surface temperature is assumed to be 273 K. Therefore, the mean drop temperature is 286 K, and the vapor properties are evaluated at 175 K. These properties, obtained from references 7 to 9, are given in table IV.

Calculating the parameters W_d, w^*, and S in equation (C25) yields

$$W_d = \frac{4\pi}{3}\rho_d R_o^3 \frac{g}{g_c} = \frac{4\pi}{3}(980)(0.0284) = 116.5 \text{ dynes} \tag{J1}$$

$$w^* = \frac{\rho u^{*2}}{g_c} R_o^2 = (0.00196)\left(\frac{1.16\times10^{-4}}{0.00196}\right)^2 \frac{R_o^2}{R_o^2} = 6.86\times10^{-6} \text{ dynes} \tag{J2}$$

$$\lambda^* = \lambda\left[1 + \frac{1}{2}\left(\frac{C_p\,\Delta T}{\lambda}\right)\right] = 198\left\{1 + \frac{1}{2}\left[\frac{(1.045)(196)}{198}\right]\right\} = 307 \text{ Joules/cm} \tag{J3}$$

$$S = \frac{1}{Pr}\left[\frac{C_p(T_d - T_s)}{\lambda^*}\right] = \left(\frac{1.76\times10^{-4}}{1.16\times10^{-4}}\right)\left(\frac{196}{307}\right) = 1.031 \tag{J4}$$

TABLE IV. - PROPERTIES OF VAPOR, WATER SPHERE,

AND LIQUID NITROGEN

Vapor properties:	
Viscosity, μ, dyne-sec/cm^2	1.16×10^{-4}
Thermal conductivity, k, W/(cm)(K)	1.76×10^{-4}
Density, ρ, g/cc	0.00196
Specific heat, C_p, J/(g)(K)	1.045
Properties of sphere:	
Thermal conductivity, W/(cm)(K):	
Liquid, k_l	0.0057
Ice, k_{ice}	0.0235
Density, g/cc:	
Sphere, ρ_d	1
Ice, ρ_{ice}	0.9
Specific heat, J/(g)(K):	
Sphere, $(C_p)_d$	4.19
Ice, $(C_p)_{ice}$	1.9
Latent heat of fusion, γ, J/g	336
Radius of sphere, R_o, cm	0.305
Properties of liquid nitrogen:	
Density, ρ_l, g/cc	0.81
Latent heat of vaporization, J/g	198
Acceleration of local gravity, g-cm/sec^2	980
Gravitational constant, g_c, g-cm/dyne-sec^2	1

$$f(\theta^*) = \cos^2\theta^* - 2\cos\theta^* + 1 = \cos 66\tfrac{1}{2}^\circ + 2\cos 66\tfrac{1}{2}^\circ + 1 = 1.956 \qquad \text{(J5)}$$

Using these values, the Nusselt number may be calculated according to equation (C25) as

$$Nu_d = \frac{h_d R_o}{k} = 1 + \left[\frac{W_d}{6\pi w^* Sf(\theta^*)}\right]^{1/4}$$

$$= 1 + \left[\frac{116.5}{6\pi(6.86\times10^{-6})(1.031)(1.956)}\right]^{1/4} = 26.8 \qquad \text{(J6)}$$

The heat-transfer coefficient is readily determined

$$h_d = \frac{k}{R_o} Nu_d = \left(\frac{1.76\times10^{-4}}{0.305}\right)(26.8) = 0.0155 \text{ watt/(cm}^2\text{)(K)} \tag{J7}$$

The average heat-transfer coefficient to a 0.6-centimeter-diameter sphere warming in a gas stream (ambient air) flowing at velocities to 1/4 meter per second was found experimentally to be approximately

$$Nu_{amb} = 10 \tag{J8}$$

Therefore, for these calculations it was assumed that

$$h_{amb} = \frac{k}{R_o} Nu_{amb} = \frac{1.76\times10^{-4}}{0.305}(10) = 0.0058 \text{ watt/(cm}^2\text{)(K)} \tag{J9}$$

The average heat transfer for the floating sphere would be dependent on the surface area exposed to gaseous nitrogen A_{amb} and that exposed to the Leidenfrost phenomenon A_{fb}

$$\bar{h} = \frac{A_{fb}}{A} h_{fb} + \frac{A_{amb}}{A} h_{amb} \tag{J10}$$

For the case of the 0.3-centimeter-diameter sphere, discussed in appendix H, where $\theta^* = 113\frac{1}{2}^o$, the heat-transfer areas become

$$A_{fb} = -2\pi R_o^2(\cos\theta^* - 1) = 4\pi R_o^2(0.7) \tag{J11}$$

$$A_{amb} = 1 - A_{fb} = 4\pi R_o^2(0.3) \tag{J12}$$

These areas are not significantly altered for the 0.305-centimeter-diameter sphere.

Substituting equations (J11), (J12), (J9), and (J7) into equation (J10) yields the average heat-transfer coefficient for the floating sphere

$$\bar{h} = (0.7)(0.0155) + (0.3)(0.0058) = 0.0126 \text{ watt/(cm}^2\text{)(K)} \tag{J13}$$

The time required to freeze a spherical shell $0.1R_o$ thick may now be determined by using equation (I21). Evaluating the constants ^1C and ^2C gives

$$^{1}C = 1 - \frac{R_o h_d}{k_{ice}} = 1 - \frac{(0.305)(0.0126)}{0.0235} = 0.837 \tag{J14}$$

$$^{2}C = \frac{R_o h_d}{k_{ice}} = 0.163 \tag{J15}$$

Before ^{3}C can be evaluated, the heat-transfer coefficient h_l must be selected. In this part of the calculation, assume it to be k_l/R_o.

$$-^{3}C = \frac{h_l(\overline{T}_d - T_f)}{\rho_{ice}\gamma R_o} = \frac{k_l(\overline{T}_d - T_f)}{\rho_{ice}\gamma R_o^2} = \frac{0.0057(286 - 273)}{0.9(336)(0.305)^2} = 0.002634 \text{ sec}^{-1} \tag{J16}$$

$$^{4}C = \frac{h_d(T_f - T_s)}{\rho_{ice}\gamma R_o} = \frac{0.0126(273 - 77)}{0.9(336)(0.305)} = 0.027 \text{ sec}^{-1} \tag{J17}$$

$$C_R = \left(^{2}C\,^{3}C\right)^2 - 4\,^{1}C\,^{3}C\,^{4}C = 0.163(-0.00263)^2 - 4(0.84)(-0.00263)(0.027)$$

$$= 2.36\times10^{-4} \text{ sec}^{-2} \tag{J18}$$

As the characteristic $C_R > 0$, equation (I21a) is applicable, or

$$t = -\frac{1}{0.00263}\left[(1 - 0.9) + \frac{0.027}{0.0154}\ln\left|\frac{(1.8)(0.837)(-0.00263) + (0.163)(-0.00263) - 0.0154}{(1.8)(0.837)(-0.00263) + (0.163)(-0.00263) + 0.0154}\right.\right.$$

$$\left.\left.\times\frac{2(0.837)(-0.00263) + (0.163)(-0.00263) + 0.0154}{2(0.837)(-0.00263) + (0.163)(-0.00263) - 0.0154}\right|\right]$$

$$= 3.7 \text{ sec} \tag{J19}$$

This is the time required for the entire sphere with a liquid core heat source to freeze a $0.1R_o$ shell.

Assume now that the sensible heat of the liquid core is negligible; the time as calculated by equation (I22) becomes

$$t = \frac{0.9(336)(0.305)}{3(0.0126)(196)} \left\{1 - (0.9)^3 + \frac{0.305(0.0126)}{2(0.0235)} \left[1 - 3(0.9)^2 + 2(0.9)^3\right]\right\}$$

$$= 3.2 \text{ sec} \qquad \text{(J20)}$$

The difference in time with and without sensible heat is about 0.5 second, about a 15 percent difference. The time required to freeze other thicknesses by these techniques is shown in figure 12.

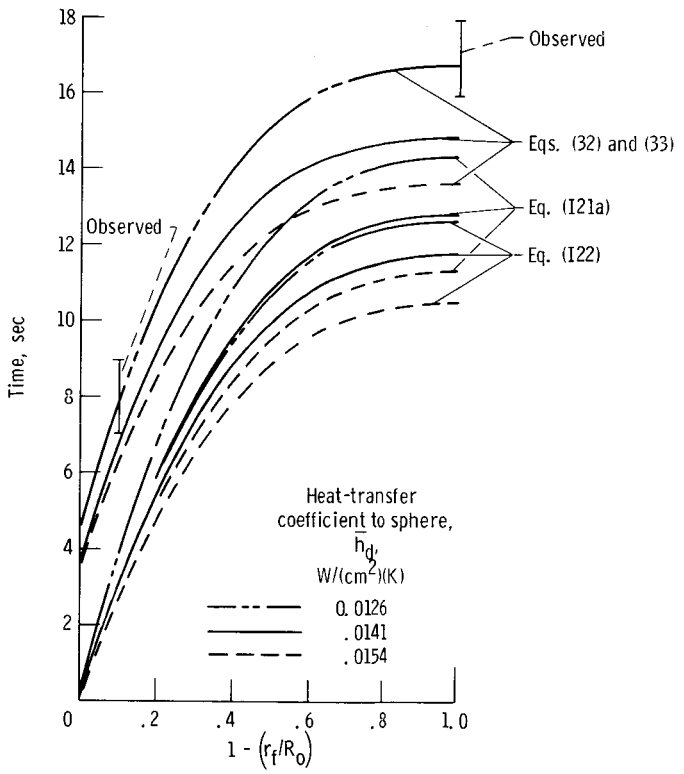

Figure 12. - Freezing interface advancement time as function of position.

The time required to obtain an $0.1R_o$ shell of ice may also be obtained through the simplified energy balance. If we let

$$t_{obs} = t_{sen} + t_{ice} \qquad \text{(J21)}$$

then the time to remove the sensible heat without any surface freezing is given by equation (32).

$$t_{sen} = \frac{m\left(C_p\right)_d (T_{d,o} - T_f)}{(hA)_d (T_f - T_s)} = \frac{(0.117)(4.19)(298 - 273)}{\left[(0.0126)(4\pi)(0.305)^2\right](273 - 77)} = 4.2 \text{ sec} \tag{32}$$

The time required to freeze the $0.1R_o$ thickness shell is given by equation (33):

$$t_{ice} = \frac{m_{ice}\gamma}{(hA)_d (T_f - T_s)} = \frac{R_o \rho_{ice}\left[1 - \left(\frac{r_f}{R_o}\right)^3\right]\gamma}{3h_d (T_f - T_s)} = \frac{(0.305)(0.9)\left[1 - (0.9)^3\right](336)}{3(0.0126)(273 - 77)}$$

$$= 3.4 \text{ sec} \tag{33}$$

Based on these estimates, the time required to freeze a $0.1R_o$ concentric shell would be (eq. (J21))

$$t_{obs} = t_{sen} + t_{ice} = 7.6 \text{ sec} \tag{J22}$$

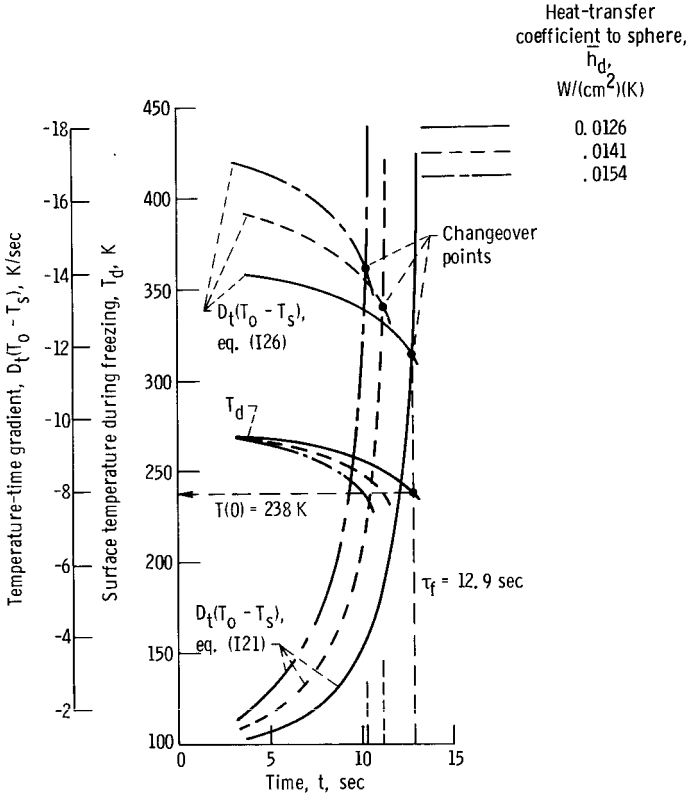

Figure 13. - Solution for changeover point from equation (I21) to equation (I26).

In comparing this time with equation (J19), it is evident that all the sensible heat cannot be extracted without freezing at the surface. These techniques are compared in figure 12 at various positions of the freezing interface.

In figure 12, it may be noted that the calculations were carried to $r_f/R_o = 0$ without regard to the changeover point as discussed in appendix I. Figure 13 illustrates the variation in the temperature-time gradients $D_t(T - T_s)$ for equations (I21) and (I26) as functions of time and surface temperature. The changeover occurs where the slopes are equal:

$$D_t\left(T - T_s\right)_{\text{eq. (I21)}} = D_t\left(T - T_s\right)_{\text{eq. (I26)}} \tag{I27}$$

The required parameters $T(0)$ and τ_f are then determined from figure 13.

$$\begin{aligned} T(0) &= 238 \text{ K} \\ \tau_f &= 12.9 \text{ sec} \end{aligned} \tag{J23}$$

To estimate the time required for the surface temperature to drop to the ordinary Leidenfrost point (i.e., the termination of the floating conditions relative to a smooth steel surface), equations (I31) and (J23) are used, with $T_L = 98$ K,

$$\tau_L = -\frac{R_o\left(\rho C_p\right)_{ice}}{3h_d} \ln\left|\frac{T_L - T_s}{T(0) - T_s}\right|$$

$$= -\frac{(0.305)(0.9)(1.9)}{(3)(0.0126)} \ln\left(\frac{20}{160.6}\right)$$

$$= 28.3 \text{ sec} \tag{J24}$$

The time from placement of the liquid-water sphere on the liquid nitrogen to the time it will sink is, from equations (I24), (J23), and (J24),

$$t_L = 12.9 + 28.3 = 41.2 \text{ sec} \tag{J25}$$

The result is in fair agreement with the data of table III.

The pseudo-steady-state analysis and the simplified energy balance techniques vary in their agreement with the data. The effects of things we do not know, such as the Leidenfrost temperature for a water sphere on liquid nitrogen, and the simplifying as-

sumptions of appendix I indicate (1) the pseudo-steady-state analysis should be modified, and (2) that the experimental data should include thermocoupled spheres to determine the Leidenfrost temperature T_L and the degree of subcooling of the sphere during freezing.

The calculations made in this appendix are summarized in table V.

TABLE V. - SUMMARY OF SAMPLE CALCULATIONS

Parameter	Calculated value	Experimental value
Sphere weight, W_d, dynes	116.5	-------
Weight for nondimensionalizing, w*, dynes	6.87×10^{-6}	-------
Sensible-to-latent-heat parameter, S	1.031	-------
Nusselt number, Nu	26.8	-------
Heat-transfer coefficient to sphere, $\bar{h}_d$, $W/(cm^2)(K)$	0.0126	-------
Pseudo-steady-state solution		
Time required to freeze a $0.1R_o$ concentric shell, t, sec:		
With sensible heat	3.7	-------
Without sensible heat	3.2	8 to 9
Time sphere will float, t_L, sec	41.2	23 to 27
Simplified energy balance		
Time require to freeze a base $0.1R_o$ thick, extracting all sensible heat first, t_{obs}, sec	7.6	8 to 9
Time sphere will float, t_L, sec	46.0	23 to 27

APPENDIX K

ESTIMATE OF LEIDENFROST TEMPERATURE

The Leidenfrost temperature is the temperature on the pool-boiling curve associated with the change from film to transition boiling. A recent, but as yet unpublished, work by Baumeister and Henry shows how large changes in the surface characteristics affect the measurement of the Leidenfrost temperature. They show that the Leidenfrost temperature of saturated water on glass is considerably higher than the Leidenfrost temperature of water on steel. These results are shown in figure 14 in terms of the temperature differences above the liquid saturation temperature.

For liquid nitrogen on a metallic surface, the Leidenfrost temperature is about 97 K, or about 20 K over the saturation temperature of nitrogen at atmospheric pressure. In this analysis, however, the Leidenfrost temperature of an ice-nitrogen combination is required. At present, there are no available data from which to estimate this Leidenfrost temperature. Consequently, an estimate of the ice-nitrogen Leidenfrost point is made from the data shown in figure 14.

First, the dimensionless Leidenfrost temperature difference θ_L for smooth or rough surfaces, shown in figure 14, is assumed to vary linearly as a function of the natural logarithm ξ/ξ_{steel}. However, the variation of ξ with surface roughness, a geometry factor, has not yet been assessed. Consequently, the superposition principle will be used herein. For smooth-surfaced ice, the ratio of ξ_{ice}/ξ_{steel} is 13.7. Consequently, the Leidenfrost temperature of smooth-surfaced ice on nitrogen will be approximately 1.89 times the value measured on steel.

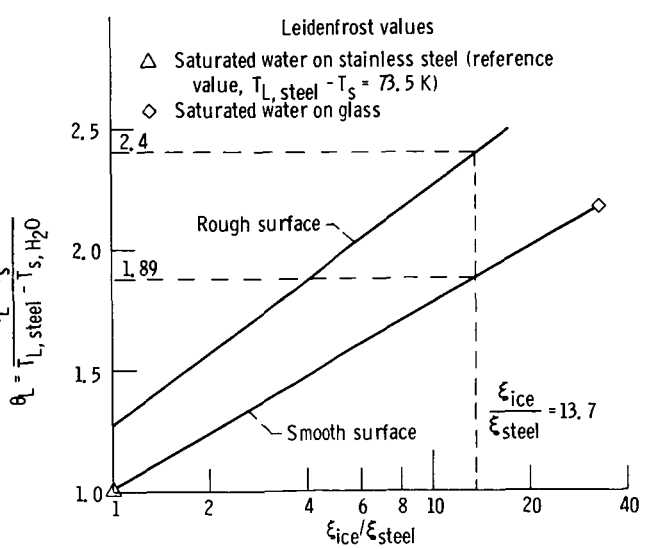

Figure 14. - Effect of surface on Leidenfrost temperature.

Besides the correction for surface properties, an additional correction for surface roughness must be considered in estimating the Leidenfrost point of an ice-nitrogen combination. The previous estimate for the Leidenfrost point assumed a smooth surface on the ice sphere. However, as was mentioned in the body of this report, ice crystal protrusions occur on the surface. Cumo, et al. (ref. 13) investigated the effect of surface roughness on the Leidenfrost point. Cumo, et al. (ref. 13) report that the Leidenfrost temperature difference for water on a smooth gold-plated surface is 285° C, while the Leidenfrost temperature difference on a sandblasted surface is 335° C. Thus, the ratio of the temperature differences for a rough to a smooth surface is 1.27.

The increase in the Leidenfrost temperature difference is a result of the decrease in the effective value of ξ at the surface due to the surface protrusions that penetrate through the vapor layer. At present, however, there is no means of estimating the new value of ξ. Consequently, it is assumed herein that the dimensionless Leidenfrost difference for a rough surface will be proportional to that measured on a smooth surface. The constant of proportionality is taken from the data of reference 13 to be 1.27. This constant is assumed to be independent of the value of ξ. Multiplying the dimensionless Leidenfrost temperature difference for the smooth surface by this value gives the upper line in figure 14 which applies for rough surfaces.

From figure 14, Leidenfrost temperature difference for the rough ice-nitrogen combination is now estimated to be 2.4 times the value measured on steel, about 126 K.

It must be emphasized that this is only a first-order estimate. The data and line shown in figure 14 do not take into account property variations of the liquid, only the metallic surface properties are considered.

REFERENCES

1. Anon.: Propellant Work Shows New Film-Boiling Aspect. Chem. Eng. News, vol. 44, Apr. 25, 1966, pp. 60-61.

1a. Alfvén, Hannes: Antimatter and Cosmology. Sci. Am., vol. 216, no. 4, Apr. 1967, pp. 106-114.

2. Baumeister, Kenneth J.; and Hamill, Thomas D.: Creeping Flow Solution of the Leidenfrost Phenomenon. NASA TN D-3133, 1965.

3. Baumeister, Kenneth J.; Hamill, Thomas D.; and Schoessow, Glen J.: A Generalized Correlation of Vaporization Times of Drops in Film Boiling on a Flat Plate. Proceedings of the Third International Heat Transfer Conference. Vol. 4. AIChE, 1966, pp. 66-73.

4. Baumeister, K. J.; Hamill, T. D.; Schwartz, F. L.; and Schoessow, G. J.: Film Boiling Heat Transfer to Water Drops on a Flat Plate. Chem. Eng. Progr. Symp. Ser., volume 62, no. 64, 1966, pp. 52-61.

5. Bird, R. Byron; Stewart, Warren E.; and Lightfoot, Edwin N.: Transport Phenomena. John Wiley & Sons, Inc., 1960.

6. Ames, William F.: Nonlinear Partial Differential Equations in Engineering. Academic Press, 1965.

7. Strobridge, Thomas R.: The Thermodynamic Properties of Nitrogen From 64 to 300° K Between 0.1 and 200 Atmospheres. Tech Note 129, National Bureau of Standards, Jan. 1962.

8. Johnson, Victor J.: A Compendium of the Properties of Materials at Low Temperatures. Phase I. National Bureau of Standards (WADD TR 60-56), July 1960.

9. McAdams, William H.: Heat Transmission. Third ed., McGraw-Hill Book Co., Inc., 1954.

10. Hendricks, Robert C.; and Baumeister, Kenneth J.: Film Boiling From Submerged Spheres. NASA TN D-5124, 1969.

11. Baumeister, Kenneth J.; Hendricks, Robert. C.; and Hamill, Thomas P.: Metastable Leidenfrost States. NASA TN D-3226, April 1966.

12. Huh, Chun; and Scriven, L. E.: Shapes of Axisymmetric Fluid Interfaces of Unbounded Extent. J. Colloid Interface Sci., vol. 30, no. 3, July 1969, pp. 323-337.

13. Cumo, Maurizio; Farello, G. E.; and Ferrari, Guiseppe: Notes on Droplet Heat Transfer. Chem. Eng. Prog. Symp. Ser., vol. 65, no. 92, 1969, pp. 175-187.

Motion-picture film supplement C-267 is available on loan. Requests will be filled in the order received.

The film (16mm, 14 min, color, sound) presents background material and discusses the forces acting to levitate a sphere in Leidenfrost boiling on a liquid interface. The associated phenomena are demonstrated by using blue-tinted water spheres floating on a sea of liquid nitrogen. As the sphere freezes, the color changes from blue to lavender and the partly frozen sphere is free to roll about on the surface because of the shift in the center of gravity. The freezing sphere crystallizes and frequently splits into two major fragments. These fragments are at first repelled and then attracted until they reattach. As time progresses, the surface temperature decreases until transition boiling begins; this destroys the vapor cushion and the sphere sinks to the bottom. Water spheres can be dropped several centimeters and still float; however, size, fluid properties, and dropping distance are important. A sequence of two floating dye-tinted spheres which attach is followed to the point where they sink.

The phenomena are again demonstrated using n-heptane. A small-scale fuel spill is simulated.

The whole process is then reversed (i.e., the liquid nitrogen is floated on water). Vapor flow patterns are very easily detected and ice paddy residues are common. The liquid-nitrogen spheres are seen to vibrate in distinct modes, and ice tracers enable the observer to follow flows internal to the liquid-nitrogen sphere.

The process is discussed as a flow visualization technique.

Film supplement C-267 is available on request to

Chief, Management Services Division (5-5)
National Aeronautics and Space Administration
Lewis Research Center
21000 Brookpark Road
Cleveland, Ohio 44135

CUT

Date _____

Please send, on loan, copy of film supplement C-267 to
TN D-5694

_____
Name of Organization

_____
Street Number

_____
City and State Zip Code

Attention: Mr. _____
Title _____

NATIONAL AERONAUTICS AND SPACE ADMINISTRATION
WASHINGTON, D.C. 20546
OFFICIAL BUSINESS

FIRST CLASS MAIL

POSTAGE AND FEES PAID
NATIONAL AERONAUTICS AND
SPACE ADMINISTRATION

POSTMASTER: If Undeliverable (Section 158 Postal Manual) Do Not Return

"The aeronautical and space activities of the United States shall be conducted so as to contribute . . . to the expansion of human knowledge of phenomena in the atmosphere and space. The Administration shall provide for the widest practicable and appropriate dissemination of information concerning its activities and the results thereof."

—NATIONAL AERONAUTICS AND SPACE ACT OF 1958

NASA SCIENTIFIC AND TECHNICAL PUBLICATIONS

TECHNICAL REPORTS: Scientific and technical information considered important, complete, and a lasting contribution to existing knowledge.

TECHNICAL NOTES: Information less broad in scope but nevertheless of importance as a contribution to existing knowledge.

TECHNICAL MEMORANDUMS: Information receiving limited distribution because of preliminary data, security classification, or other reasons.

CONTRACTOR REPORTS: Scientific and technical information generated under a NASA contract or grant and considered an important contribution to existing knowledge.

TECHNICAL TRANSLATIONS: Information published in a foreign language considered to merit NASA distribution in English.

SPECIAL PUBLICATIONS: Information derived from or of value to NASA activities. Publications include conference proceedings, monographs, data compilations, handbooks, sourcebooks, and special bibliographies.

TECHNOLOGY UTILIZATION PUBLICATIONS: Information on technology used by NASA that may be of particular interest in commercial and other non-aerospace applications. Publications include Tech Briefs, Technology Utilization Reports and Notes, and Technology Surveys.

Details on the availability of these publications may be obtained from:

SCIENTIFIC AND TECHNICAL INFORMATION DIVISION

NATIONAL AERONAUTICS AND SPACE ADMINISTRATION

Washington, D.C. 20546